Hindawi
Geofluids
Volume 2023, Article ID 3969979, 22 pages
https://doi.org/10.1155/2023/3969979

Research Article

Morphology and Depositional Processes of a Carbonate-Filled Canyon in the Carboniferous KT-II Formation of the Eastern Precaspian Basin, Kazakhstan: Insight from 3D Seismic Data

Jiapeng Wu,[1] Xiaodong Cheng,[1] Shanbo Sheng,[2] Leyuan Fan,[1] Kai Guo,[1] Xining Li,[1] Wan Diao,[3] Unmei Tai,[1] Shutang Jin,[2] Shengbin Zhang,[1] and Xinxin Song[4]

[1]*China National Logging Corporation, CNPC, Beijing 100101, China*
[2]*Aktyubin Oil/Gas Ltd., CNPC, Aktyubin 030000, Kazakhstan*
[3]*Geological Research Center, GRI, BGP Inc., CNPC, Zhuozhou 072750, China*
[4]*Geology Research Institute, Greatwall Drilling Company, CNPC, Panjin 124010, China*

Correspondence should be addressed to Xining Li; lixining.cnlc@cnpc.com.cn

Received 6 January 2023; Revised 3 August 2023; Accepted 30 August 2023; Published 5 October 2023

Academic Editor: Mercè Corbella

Canyons in carbonate depositional settings, as important elements of the source-to-sink system, remain poorly studied compared to those in siliciclastic depositional environments. The latest high-resolution three-dimensional seismic data, well logs, and core data at the eastern edge of the Precaspian Basin are used to investigate the geomorphology, infillings, and depositional process of a unique carbonate-filled canyon in the Carboniferous KT-II formation parallel to the carbonate platform, which is distinct from other slope-perpendicular canyons. The canyon has a total length of more than 52.3 km with a nearly N-S orientation and an S-shaped geometry, and the whole canyon can be divided into three segments by two knickpoints. The slope-parallel orientation of the canyon is mainly controlled by the palaeogeomorphology and reverse faults. Due to the collision of the Kazakh and European plates in the early-middle Visean (early Carboniferous), the canyon was formed in a northern tilted, elongated, and restricted palaeotopographic feature between uplifts. The development of reverse faults related to tectonic movement controlled the variations in the width of the canyon and the positions of the knickpoints. Tectonics controlled the orientation and formation of the canyon, while sedimentary processes contributed to its infilling. The well-seismic tie analysis indicated two distinct periods of the canyon fillings, Ss1 and Ss2, which were separated by a second-order sequence boundary. The lower part contained sediments supplied by both sides of the canyon through channels or gullies, and the upper part was dominated by a carbonate platform that prograded from the eastern side of the canyon. The evolution of the canyon can be subdivided into three stages. The increasing stage was mainly characterized by significant upslope erosion through headward retrogressive mass failures in the slope-parallel confined negative relief to form the canyon during the lowstand system tract of Ss1. Subsequently, in the early filling stage, the carbonate factory was productive during the highstand, and massive excess carbonate sediments were transported into the adjacent canyon by channels or gullies on both sides and deposited. The canyon was basically filled, and the morphology became much gentler. During the subsequent late filling stage, the carbonate platform was flooded again during the highstand, and the production rates of the carbonate factory greatly increased. The lateral progradation of carbonate platforms accelerated on the canyon of the early filling stage and further into the inner sag.

1. Introduction

Submarine canyon systems, as major conduits for transporting sediments in both siliciclastic and carbonate environments [1–5], have been widely studied for their tectonic movement, sedimentary information, and climate signals, which were recorded during the evolutionary history of the canyon [1, 6–10], as well as significant amounts of hydrocarbon reservoirs discovered within canyon fillings [11, 12].

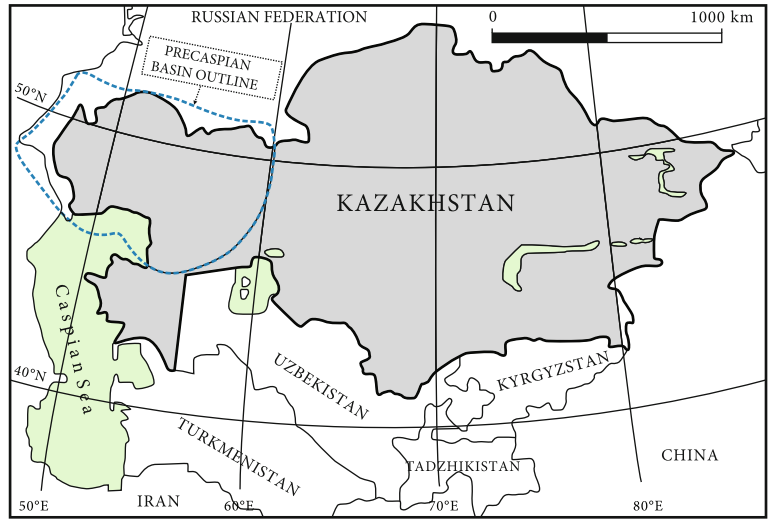

Figure 1: Schematic location map showing the outline of the Precaspian Basin in western Kazakhstan (modified after Barde et al. [37]).

Among numerous former studies, canyons in siliciclastic settings have drawn more attention [13, 14], whereas submarine canyons in carbonate depositional environments remain relatively poorly documented [14]. Due to the downslope gravity processes, most of the reported canyons are perpendicular or oblique to the slopes [7, 13, 15, 16]. Owing to some special geological settings, canyons may run parallel to slopes, for example, the Central Canyon in the Qiongdongnan Basin of the South China Sea [17–21]. However, canyons parallel or subparallel to the slope in carbonate sedimentary environments have rarely been reported. Canyons in carbonate settings are always characterized by using multibeam bathymetry [15, 22], two-dimensional (2D) seismic lines [23–27], and outcrops [28–30]. Thus, it is rarely possible for former studies to demonstrate the depositional process of the canyon as a whole sedimentary unit with a combined analysis of geomorphic features and sediment fillings. Carbonate canyons are far less understood [14, 30]. With improvements in seismic techniques and seismic image resolution, especially for the three-dimensional (3D) seismic analysis used for canyon studies, the morphology, depositional elements, and depositional dynamics of submarine canyons have been greatly enhanced [17, 31–36].

The present study takes a canyon that extends parallel to the open carbonate platform as the study object and uses high-resolution 3D seismic data, well logs, and core data to document the geomorphology, infillings, and depositional process of the Carboniferous carbonate-filled canyon (CFC). Studying this canyon is interesting because this buried canyon is completely filled with carbonate, it is parallel to the open carbonate platform, and, in contrast to other canyons connecting the continental shelf and the slope, this canyon formed in the inner sag inside the shallow open carbonate platform.

2. Geological Setting

The Precaspian Basin, located in the southeast Eastern European craton (Figure 1), is a large elliptical basin covering more than 5×10^5 km^2. In the west and north, the basin is adjacent to the Russian platform. It is bounded to the South Emba fold belt and the Karpinskiy fold zone to the south and southeast, respectively, and the eastern boundary is the south end of the Ural fold belt [37–39] (Figure 2). The tectonic evolution of the Precaspian Basin involved [40] rifting during the Devonian, [1] passive and transform continental margins of palaeocontinents during the Carboniferous, and [2] plate collisions (European, Kazakh, and Turan plates) at the end of the Permian [37, 41, 42] (Figure 3).

During basin evolution, very thick sediments were deposited in the Precaspian Basin starting in the Middle Devonian. The sedimentary strata of the basin can be divided into two major packages (presalt and postsalt), separated by the Kungurian salt [37] (Figure 3). At the end of the early Permian, the European plate collided with the Kazakh plate to the east (Ural Mountains orogeny), and then, the Precaspian Basin progressively became isolated from the open sea, leading to the deposition of a considerable amount of evaporites, i.e., the Kungurian salt (Figure 3). The presalt succession reached a depth of approximately 6000 m towards the west, which is a westerly dipping ramp [37]. In the study area, in the eastern part of the Enbeksk-Zharamysskaya Uplift, the presalt succession is mainly composed of platform carbonate units and clastic sediments deposited from the mid-Devonian to early Permian [43, 44] (Figure 3). The collision started in the late Visean, early Carboniferous, which gradually changed the deposition from passive continental margin clastic deposition to carbonate deposition [37, 38, 45] (Figure 3).

The Carboniferous stratum, the main component of presalt carbonate strata, can be divided into three lithological assemblages upwards, which are the KT-II, MKT, and KT-I formations (Figure 3). The target interval of this work is the KT-II formation, which is a set of platform carbonate deposits comprising numerous shallowing-upward parasequences. On the eastern margin of the Precaspian Basin, the main sedimentary facies of KT-II are open platform facies and restricted platform facies, and the main sedimentary microfacies include shoal, tidal channel, intershoal, and

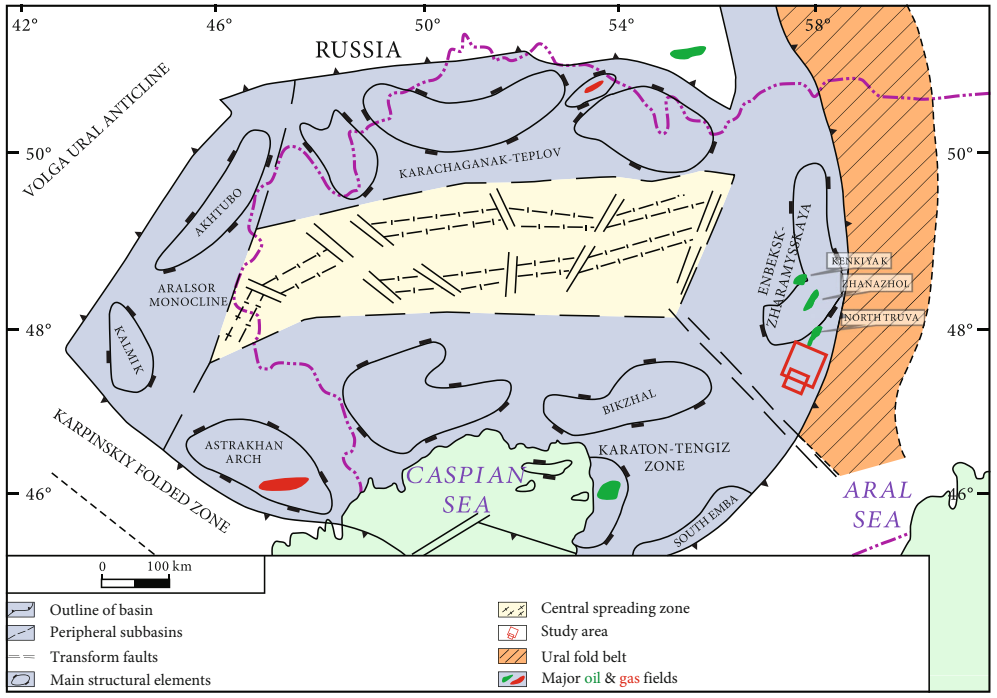

Figure 2: Map displaying the tectonic units of the Precaspian Basin (modified after Barde et al. [37] and Wang et al. [42]) and red rectangles representing the regional location of the 3D seismic surveys in this study.

lagoon microfacies [47–49]. During the deposition of KT-II, in the late Visean-early Moscovian, from the Zhanazhol oilfield to the study area, on the eastern edge of the Enbeksk-Zharamysskaya Uplift, there was a long strip-shaped, N-S-extending open carbonate platform, with the Ural trough to the east and the platform inner sag to the west [42, 46–49] (Figures 2 and 4).

3. Data and Methods

The data utilized in this study were provided by the Aktyubin subsidiary of China National Oil and Gas Exploration and Development Company Ltd. (CNODC), including two 3D seismic volumes with an area of 2000 km^2, well logs, core data, and lithological data from four exploration wells. To eliminate the influence of salt on seismic imaging of presalt strata, the seismic data of this area were processed by prestack depth migration (PSDM). The dominant frequency of the seismic data is approximately 30 Hz, with a vertical resolution of 50 m and a bin spacing of 25 m × 25 m. All vertical scales of the seismic profiles shown in this paper are in units of depth.

The PSDM seismic profiles were used for seismic-well ties to determine the key seismic reflections (the top interface of KT-II, the bottom of KT-II, the top of MKT, etc.) and canyon deposits, which were discerned through seismic facies (amplitude, frequency, and continuity) and seismic reflection termination (on-lap, downlap, truncation, etc.) (Figures 5(a)–5(f)). All these discontinuities were traced in the whole study area. The seismic data were interpreted, and the coherence slices were generated using the Seiswork module of LandMark 5000. The PostStack/PAL module in LandMark 5000 was utilized to obtain seismic data flattened along horizon, RMS, and coherence attribute maps along the horizon. In addition, the 3D visualization module in Petrel 2015 was used to generate the topographic map of the CFC and palaeogeomorphologic map of KT-II.

To accurately express geomorphic features of the CFC, many lines were used to measure the thalweg depth, width, etc., to determine parameters such as the sinuosity and thalweg slope gradient of the canyon (Figure 4). Referring to the quantitative methods used by Catterall et al. [50] and Liang et al. [20], intensive measurements were carried out for places where the local geomorphic features changed dramatically.

To calculate the sinuosity and slope gradient, the formulas of Huang et al. [51] were applied. The main formulas and data are shown as follows:

$$S_n = \frac{TL}{HtFD},$$
$$HtFG = \arctan\left(DR \times HtFD\right) \times \frac{180}{\pi}, \quad (1)$$

where S_n is the sinuosity, TL is the thalweg length, HtFD is the head-to-foot distance, HtFG is the head-to-foot gradient, and DR is the depth range.

4. Results

4.1. Geomorphology of the Canyon. The CFC in this study is located in the inner sag in the western part of the KT-II open carbonate platform (Figure 4). The CFC is more than 50 km long, 100-400 m deep, and approximately 1-5 km wide (Figure 6), the dimensions of which are similar to those of the canyons along the slopes of isolated carbonate platforms in the Xisha Archipelago [52]. Based on the quantitative measurement of the depth, width, and sinuosity, the CFC in the

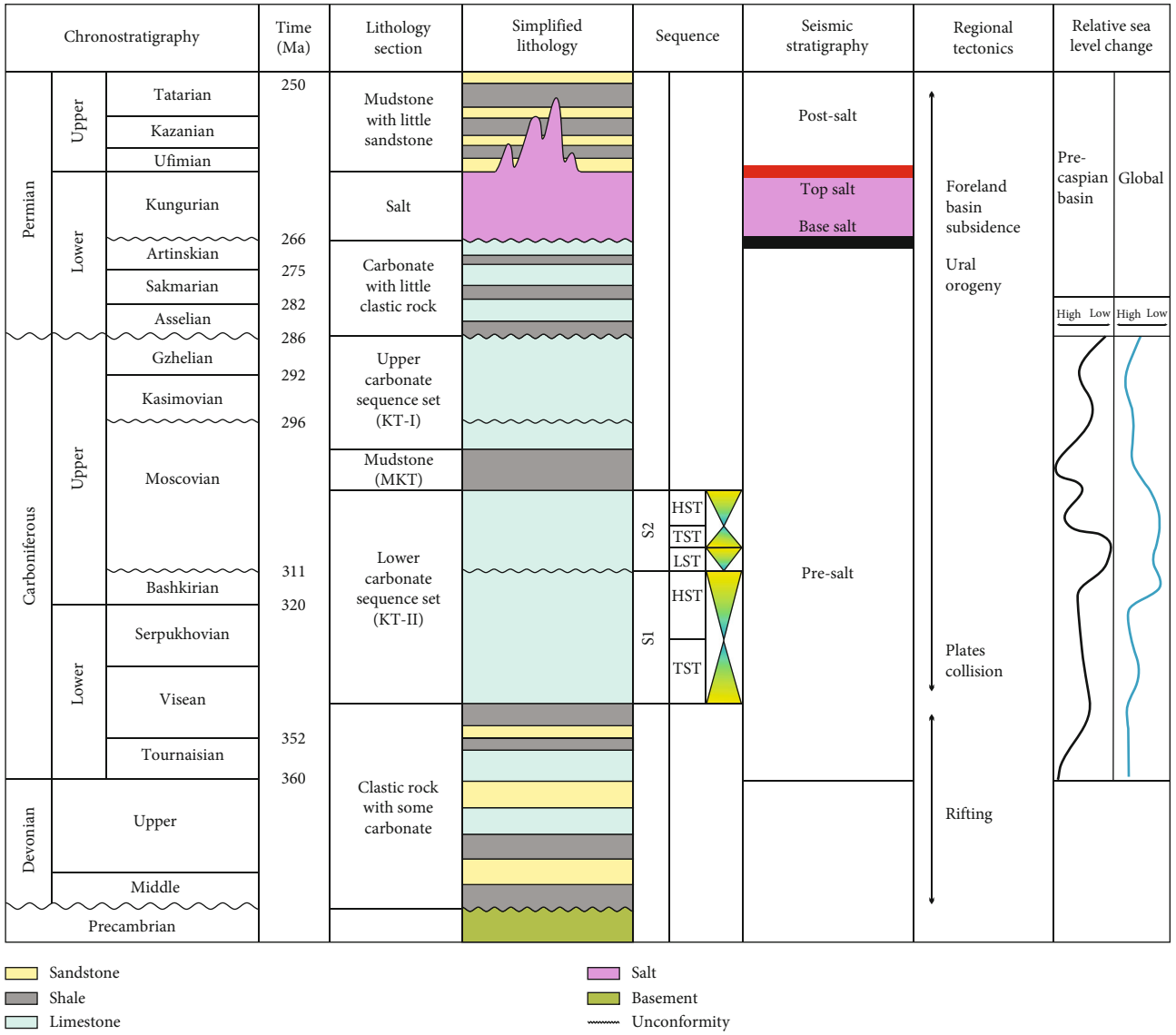

Figure 3: Stratigraphic framework, simplified lithological column, temporal intervals, main geological events, and relative sea level in the southeastern Precaspian Basin (modified after Barde et al. [37], Zhang [46], and Fernandez et al. [41]). KT-II consists of two second-order sequences, Ss1 and Ss2, and the deposition of KT-II is closely connected with plate collision.

study area was subdivided into three segments, i.e., (i) head segment, (ii) middle segment, and (iii) lower segment, by two obvious knickpoints where the CFC became narrower and the thalweg slope was steeper [53, 54]. The head segment is the first 20 km, and the lower segment is located between 35.8 and 52.3 km. The middle segment, from 20 to 35.8 km, is the shortest segment of the CFC in the study area. In plan view, the CFC shows an overall N-S extension, which is generally parallel to the KT-II open carbonate platform, an S-shaped geometry, and a generally gentle ramp along its thalweg slope profile (Figures 4 and 5(e)). To quantify the geomorphology of the CFC, the first measurement line at the southernmost end of the study area was taken as the starting point of the CFC (Figure 4). The 46.5-52.3 km interval of the northernmost section of the CFC was not fully covered by 3D seismic data, and the geomorphological characteristics of this part were not described (Figures 4 and 6(c)).

In the head segment, which is the narrowest and straightest segment, the CFC has a SSW to NNE trend and is slightly sinuous (with a sinuosity of 1.01°) (Figure 6(c)). Over the first 17.71 km, the thalweg slope is 1.11°, and the depth (from 95 m to 295 m deep) and width (from 1.48 km to 2.83 km wide) of the canyon gradually increase with little fluctuation (Figures 6(a) and 6(b)). However, between 17.71 and 20 km, a concave-up section of the thalweg profile at approximately 4.01° was observed (Figures 6(a) and 6(b)). The width and depth of the CFC decreased significantly to 1.1 km and 85 m, respectively (Figures 6(a) and 6(b)). The knickpoint of the steep slope at 20 km is knickpoint 1 (K1), which is the boundary between the head segment and middle segment, after which point the thalweg slope becomes steep and the depth of the canyon increases rapidly (Figures 5(e) and 6(c)).

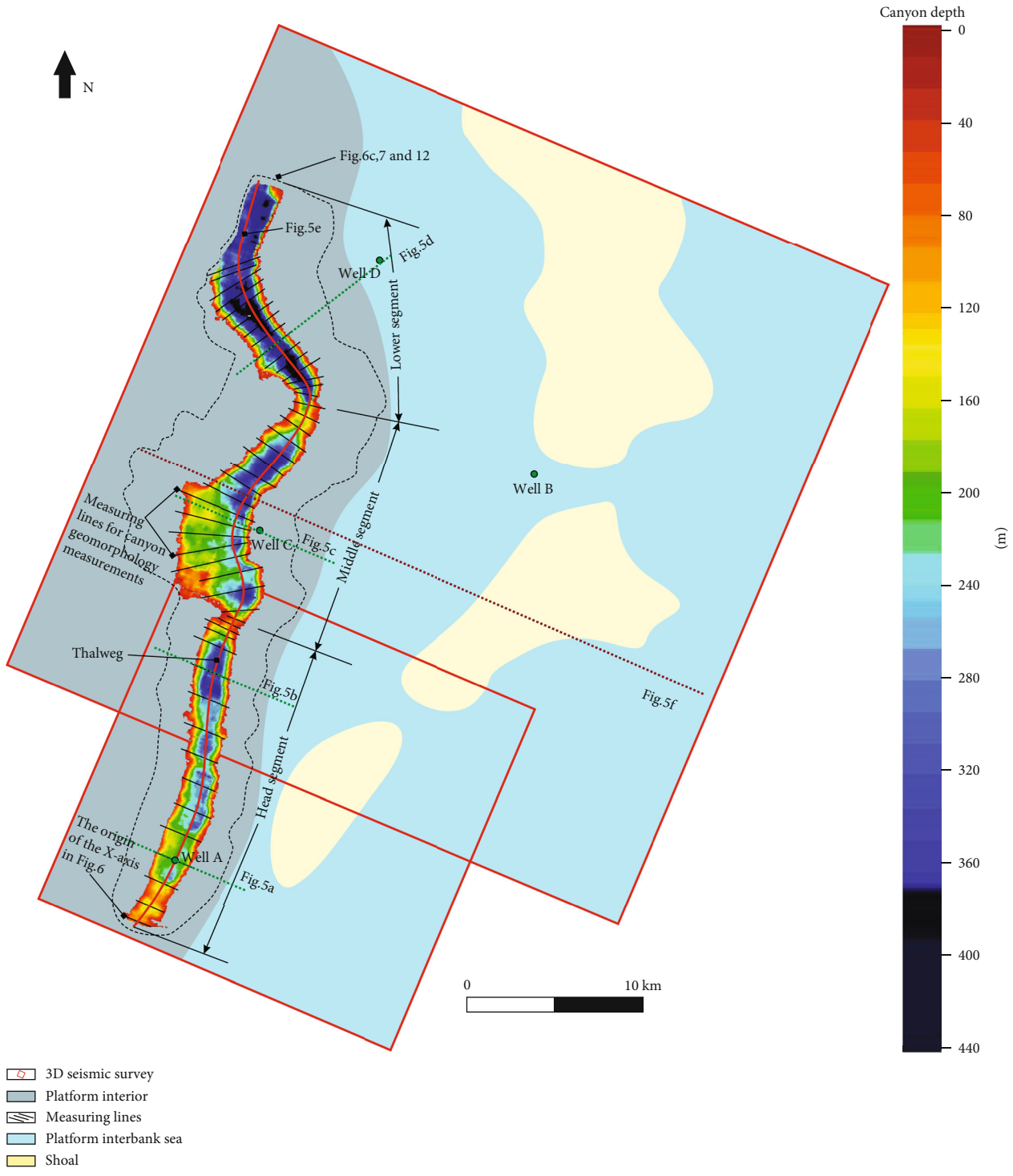

FIGURE 4: Sedimentary palaeogeographic map of KT-II in the study area (modified after Zhang [46]). Additionally, topographic map showing the geomorphology of the canyon, the locations of wells used in this study (the green dots) and the measuring lines, and the areas of the head, middle, and lower segments of the canyon. The black dotted lines illustrate the positions of Figures 6(c), 7, and 12.

The middle segment, which is the widest segment on average, is slightly S-shaped in plan view and has an overall SW-NE orientation with a sinuosity of 1.12°. From 20 to 27.4 km, the CFC trends NW and then changes abruptly to NE at 27.4 km. Within the initial part of the middle segment (20-20.7 km), the thalweg slope is the steepest of the entire study area, at approximately 17.69°, and the depth (from 80 m to 230 m deep) and width (from 1.1 km to 2.26 km wide) of the CFC increase rapidly in a short distance, similar to a "waterfall" in the canyon. Throughout the adjacent part downslope of the CFC (20.7-32.3 km), with the thalweg slope at approximately 1.95°, constant increases in the depth

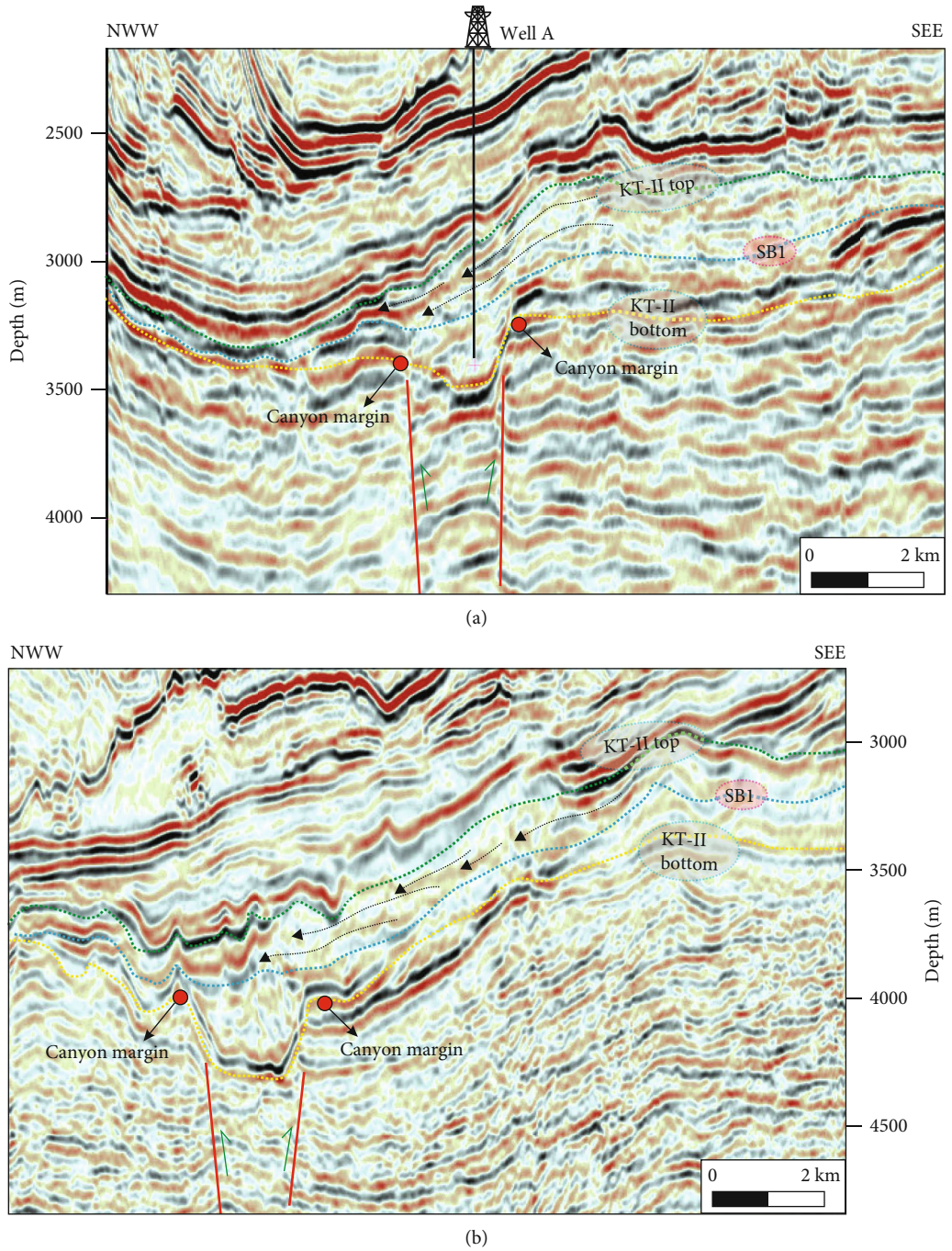

Figure 5: Continued.

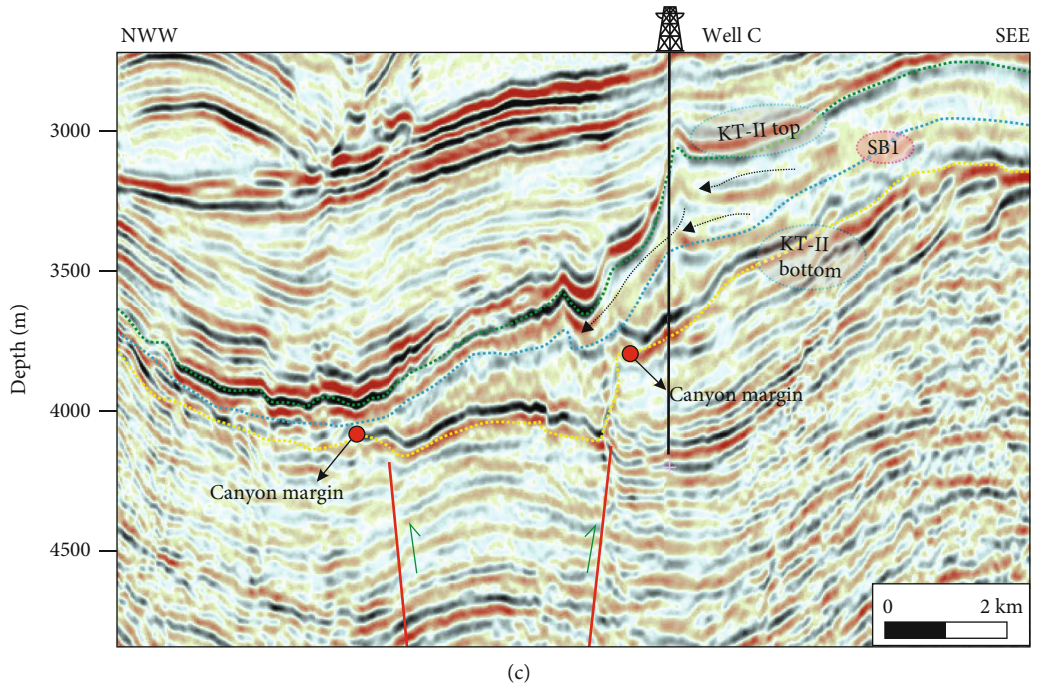

(c)

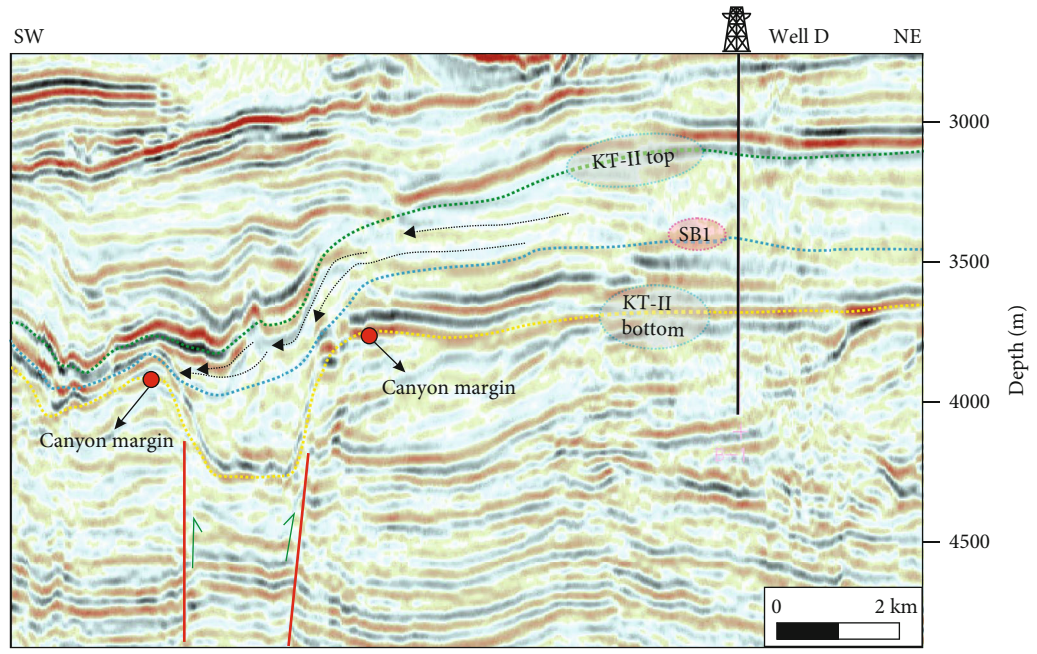

(d)

Figure 5: Continued.

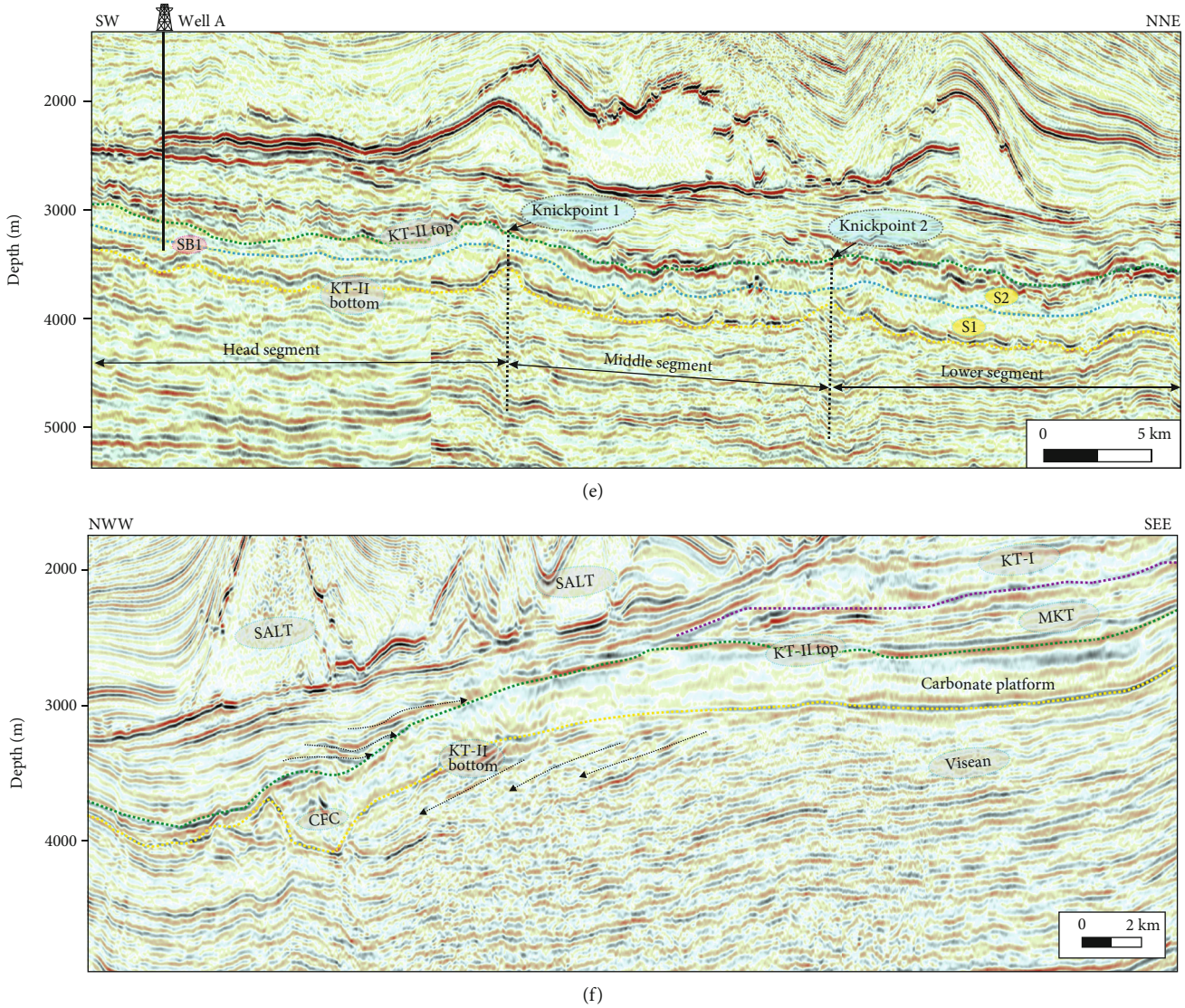

Figure 5: (a–d) Seismic profiles of the head segment (a, b), middle segment (c), and lower segment (d) (green dotted lines in Figure 4) of the canyon, showing the morphological features of the canyon in different segments. The head segment is the narrowest, the middle segment is the widest, and the lower segment is the deepest. See the text in Section 4.1 for detailed descriptions. The relationship between reverse faults and the canyon is shown. (e) Seismic profiles along the canyon thalweg (red line in Figure 4), showing that the canyon is generally a gentle ramp. Two knickpoints with abrupt morphologic changes subdivide the canyon into three segments. (f) Vertical seismic profile (red dotted line in Figure 4) across the study area, showing the distribution of canyons and carbonate platforms.

and width of the canyon are observed (Figures 6(a) and 6(b)). In the first 6.7 km of this part, the width increases rapidly (from 2.26 km to 5.12 km wide), reaching a width of 5.12 km at 27.4 km, while in the following 4.9 km, the depth increases rapidly (from 175 m to 360 m deep), reaching a depth of 360 m at 32.3 km of the CFC (Figures 6(a) and 6(b)). Similar to the head segment, a concave-up section of the thalweg longitudinal profile at approximately 2.92° is also observed between 32.25 and 35.8 km. The depth (from 260 m to 185 m deep) and width (from 2.93 km to 1.92 km wide) of the CFC decrease rapidly throughout the remaining part of the middle segment (Figures 6(a) and 6(b)). The vertex of this concave-up section at 35.8 km is knickpoint 2 (K2), marking the boundary between the middle segment and the lower segment (Figures 5(e) and 6(c)).

In the lower segment, the canyon is S-shaped in plan view with the gentlest thalweg slope and highest sinuosity of 1.17° among the three segments (Figure 6(c)). In the downstream direction from 35.8 km to 46.5 km, it trends NW and then changes abruptly to NNE at 46.5 km, with an overall SE-NW orientation of this segment (Figures 6(a) and 6(b)). Between 35.8 and 36.4 km, another "waterfall" with a steep thalweg slope of approximately 15.66° is observed. Similar to the middle segment, the CFC depth (from 185 m to 355 m deep) increases rapidly in this short section (Figures 6(a) and 6(b)). Throughout the remaining part of the lower segment, from 36.4 km to the end of the canyon in the study area, overall increases in the depth (from 355 m to 415 m deep) and width (from 1.78 km to 3.45 km wide) of the CFC are present (Figures 6(a) and 6(b)).

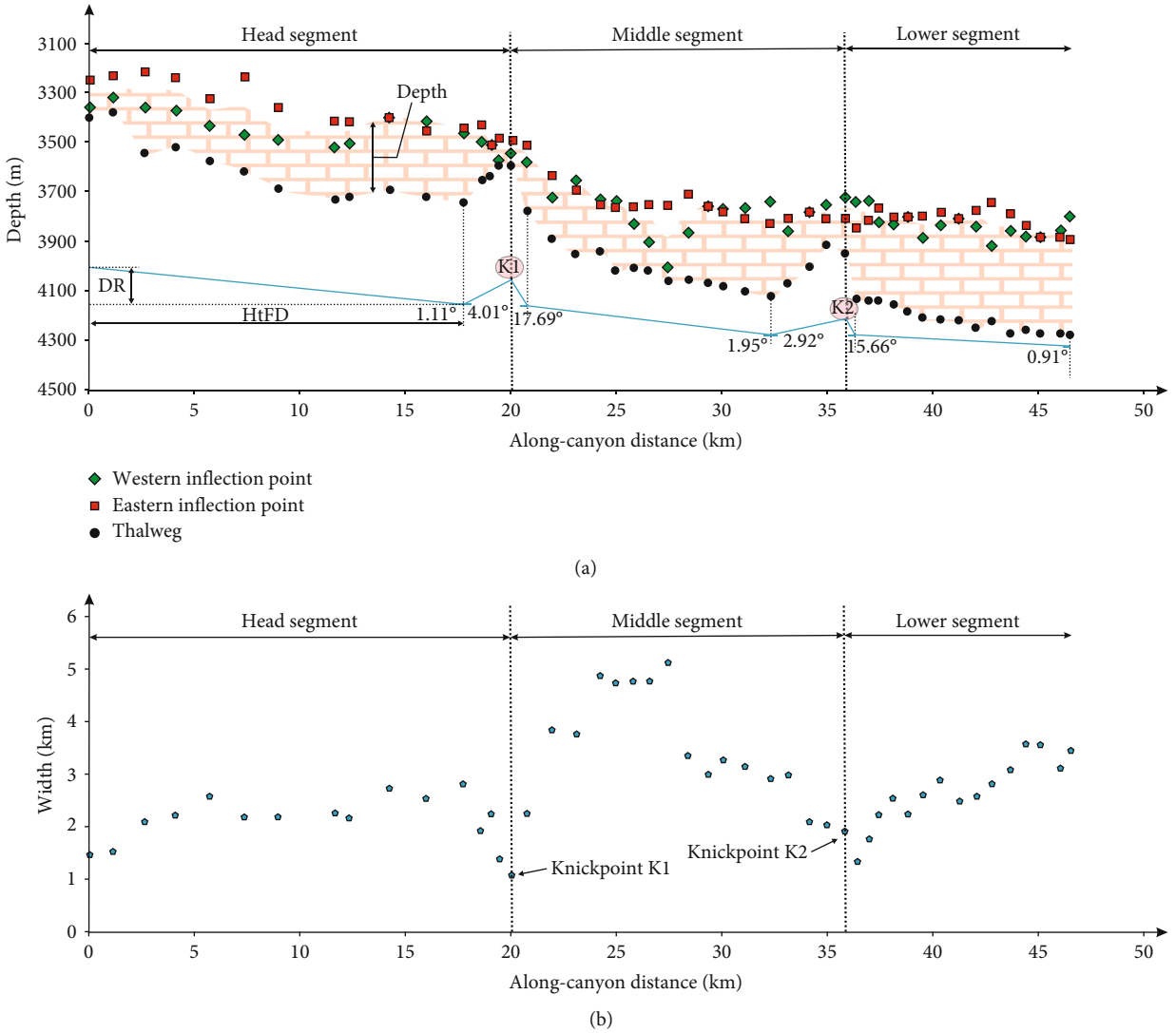

Figure 6: Continued.

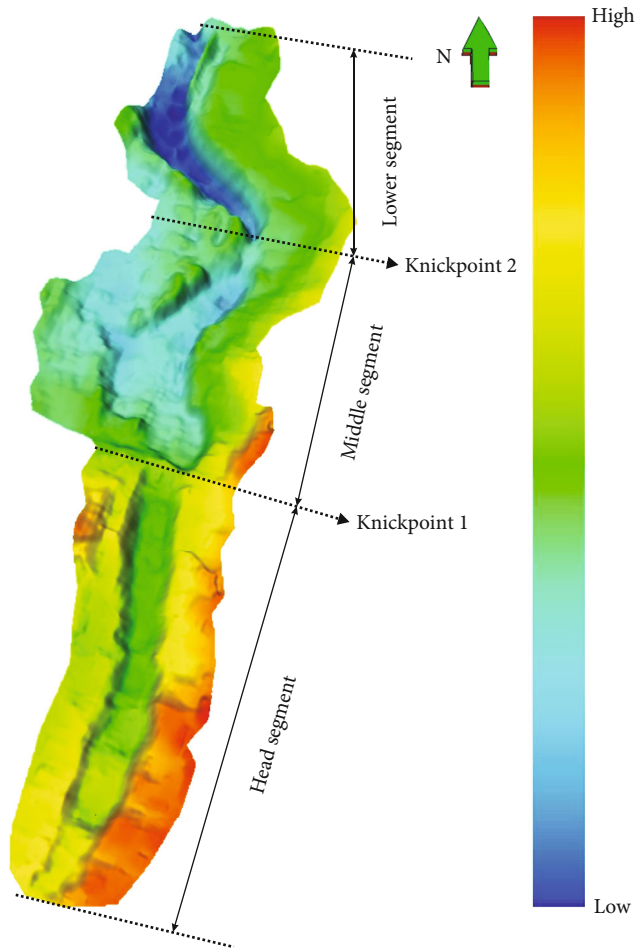

(c)

Figure 6: Measurement results of the quantification of the studied CFC geomorphology. The CFC thalweg in the first measuring line, which is in the southwestern-most corner of the study area, is referred to as the origin of the X-axis (see the supplementary Figure_6_data.pdf). (a) Vertically exaggerated plot displaying changes in the thalweg slope gradient and in the CFC depth along the mapped length of the studied canyon. (b) Vertically exaggerated plot showing changes in the CFC width along the mapped length of the studied canyon. (c) 3D view of the studied CFC, focusing on the change in the canyon depth and width among the three segments of the canyon (see the location in Figure 4).

4.2. Seismic Facies and Depositional Interpretations Associated with the CFC. Six kinds of seismic facies associated with the CFC were identified based on the external geometry and internal configuration and texture, such as the amplitude, frequency, and continuity of seismic reflection (Figures 7–9 and Table 1). Seismic facies were then calibrated and tied to different depositional elements based on the well logs and lithological data collected from several exploration wells (Figures 8 and 9).

Seismic facies 1 is interpreted as canyon fill deposits. The lithological data and gamma ray (GR) log from well A indicate mainly thick limestone with thin-bedded argillaceous limestone and marlite (Figure 9(a)). Seismic facies 2 is interpreted as platform slope deposits. The lithological data and logs from well A reveal three coarsening-upward successions, each composed of lower argillaceous limestone and marlite and upper limestone (Figure 9(a)). Seismic facies 3 is interpreted as aggrading carbonate platform deposits (Figures 9(b) and 9(e)–9(i)). The associated deposits are commonly sheet-like, and internal reflectors are parallel and straight to slightly wavy. According to the well logs and lithological data from well B, this seismic facies is pure thick limestone. Bachtel et al. [55] reported similar facies and deposits in the carbonate platform offshore Indonesia. Seismic facies 4 is a progradational carbonate platform (Figures 9(c) and 9(g)–9(k)). These are prograding platform clinoforms associated with the platform margin, reef flat, and platform interior facies indicated by offlapping reflections. Referring to the well logs and lithological data from well C, the main lithology is limestone with a thin layer of lime mudstone. Seismic facies 5 is a delta front deposit, as has been verified by the results from seismic-well ties. The GR value in well C is relatively high, reflecting the muddy sedimentary background, in which the thin box- or funnel-shaped GR log represents fine sand or silty sand deposition (Figures 9(c), 9(l), and 9(m)). Seismic facies 6 is composed of muddy shelf deposits. According to well D, the GR log is straight with high values, and the lithofacies is mainly mudstone with thin layers of fine sand or siltstone (Figure 9(d)).

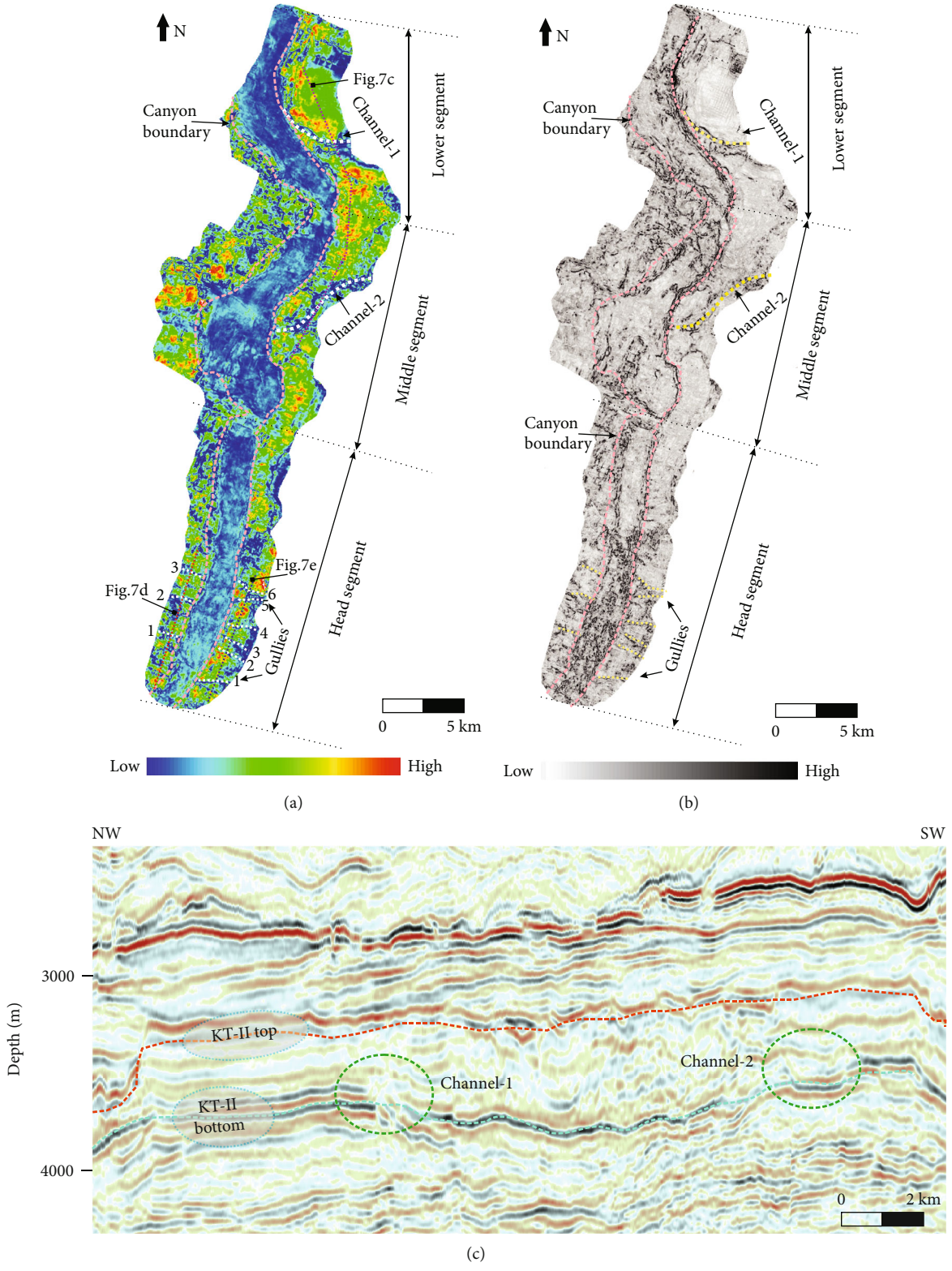

Figure 7: Continued.

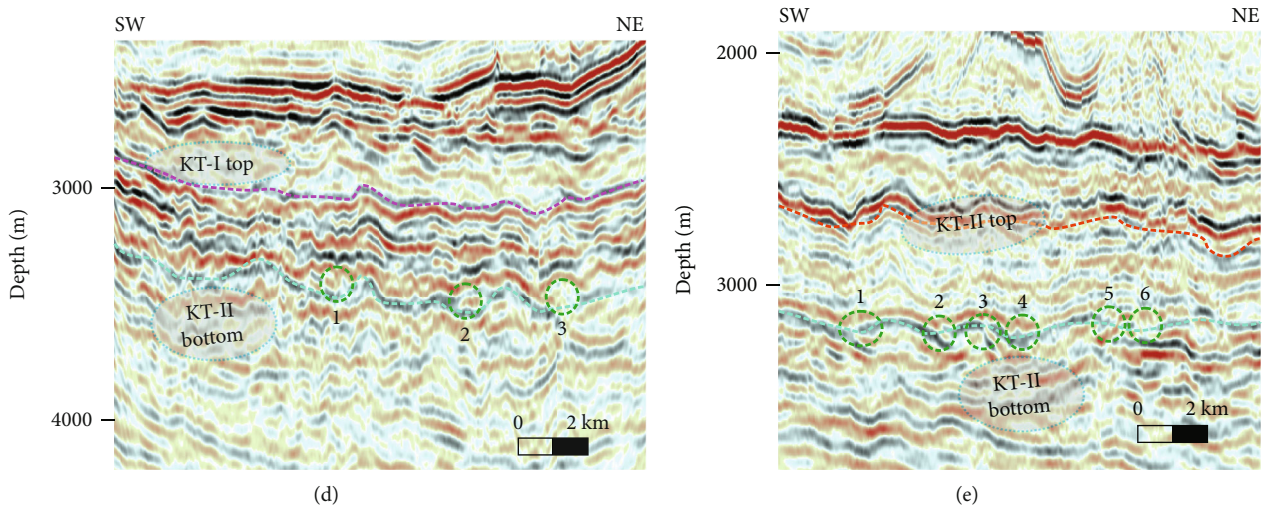

Figure 7: (a) RMS amplitude map of the CFC. The canyon filling deposits are dominated by low RMS values, while both flanks of the canyon are dominated by high RMS values. A series of small gullies are located in the head segment of the canyon, and two channels are located in the middle and lower segments, with low RMS amplitude values. (b) Coherence map along the canyon bottom. The canyon boundaries, gullies, and channels display dark-coloured coherence patterns, whereas the canyon filling deposits exhibit light-coloured coherence patterns. See the position in Figure 4. (c) Two channels of the carbonate platform in the seismic profile show chaotic weak amplitudes. See the position in (a) (purple dotted line). (d, e) Several gullies of the carbonate platform in the seismic profiles on both sides of the CFC's head segment show weak amplitudes and chaotic features with concave shapes, which are narrower and shallower than the channels. See the position in (a) (red and blue dotted lines).

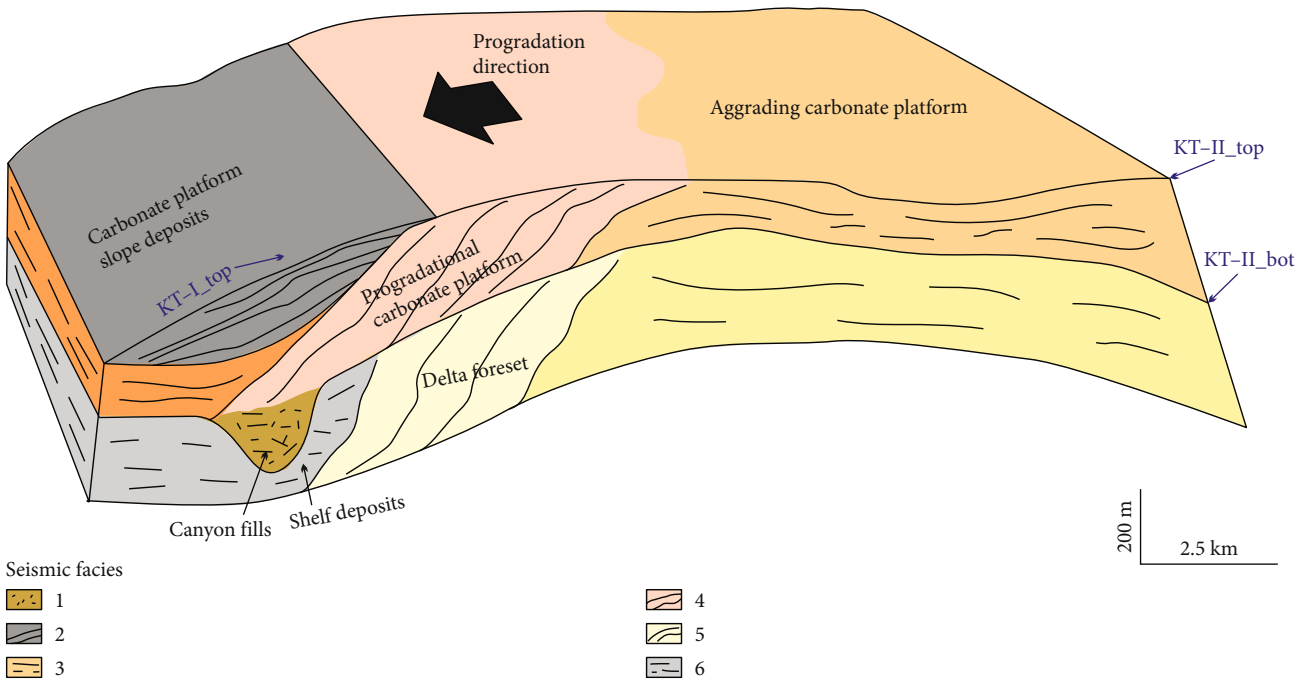

Figure 8: 3D distribution chart of six seismic facies in different locations around the studied CFC. Descriptions of the seismic facies are in the text and in Table 1.

4.3. Sequence Stratigraphic Correlation between the CFC and Platform. The current study integrates seismic and well data to investigate the sequence stratigraphic correlation between canyon infillings and platform deposition according to sequence stratigraphy, with the chronostratigraphic approach, which emphasizes studying rock units bounded by time lines [56].

To determine the relationship between the carbonate platform and the CFC, the carbonate platform strata were correlated and contrasted with the canyon infill deposits on a second-order sequence scale considering seismic resolution (Figures 5(c) and 5(d)). According to the results of the sequence stratigraphic study of the wells and seismic-well ties, the studied KT-II strata, which are mainly

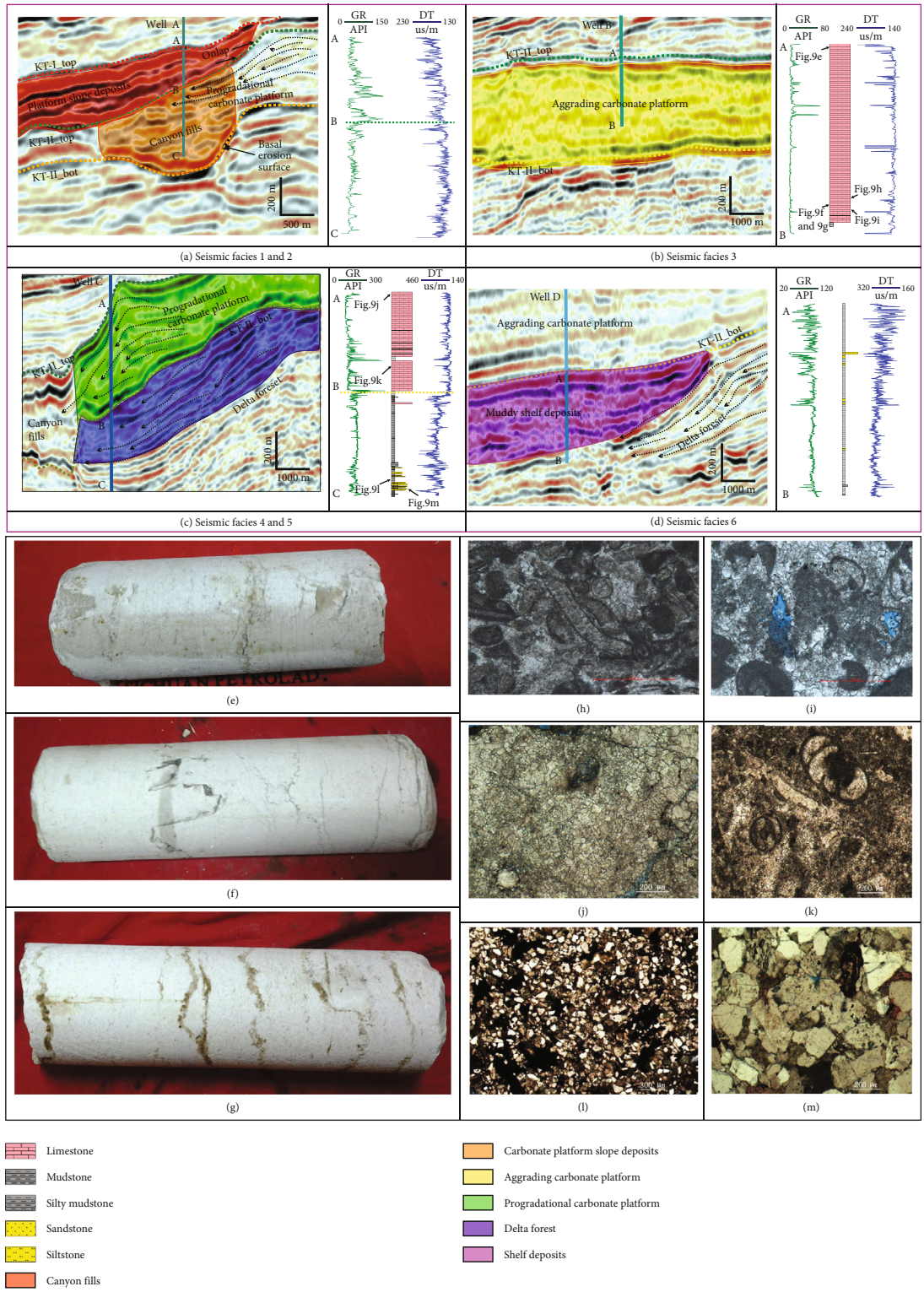

Figure 9: Seismic profiles showing six seismic facies found in the studied CFC and proximal strata. (a–d) Six seismic facies. (e–g) Core photographs of the aggrading carbonate platform (seismic facies 3 in (b)) of well B, mainly grey limestone. (h–k) Thin section photographs of carbonate platform facies in KT-II. (l, m) Thin section photographs of Visean delta foresets. (h) Sparry algal foraminiferal limestone of the aggrading platform (seismic facies 3 in (b)) in well B. (i) Sparry foraminiferal oolitic limestone of the aggrading platform (seismic facies 3 in (b)) in well B. (j) Sparry clastic limestone of the progradational platform (seismic facies 4 in (c)) in well C. (k) Sparry foraminiferal limestone of the progradational platform (seismic facies 4 in (c)) in well C. (l) Fine-grained feldspar lithic sandstone of delta foresets (seismic facies 5 in (c)) in well C. (m) Medium-grained feldspathic quartz sandstone of delta foresets (seismic facies 4 in (c)) in well C.

Table 1: Seismic reflection feature table of six seismic facies found in the studied CFC and proximal strata.

Seismic facies	Reflection orientation	Reflection continuity	Frequency	Amplitude	External geometry	Interpretation
1	Chaotic, subparallel	Moderate to low	Moderate to low	Moderate to low	U-shaped	Canyon fills
2	Parallel	High	High	High	Sheet	Carbonate platform slope deposits
3	Parallel, subparallel	High	Low to moderate	Moderate to low	Sheet	Aggrading carbonate platform
4	Inclined	Moderate	Low to moderate	Moderate to low	Wedge	Progradational carbonate platform
5	Inclined	High	High to moderate	High to moderate	Wedge	Delta foreset
6	Parallel, subparallel	High to moderate	High	Moderate	Sheet	Shelf deposits

composed of canyon fill and carbonate platform deposits, consist of two second-order sequences, Ss1 and Ss2. Each of the second-order sequences includes a lowstand system tract (LST) and a transgressive system tract (TST) in the lower part and a highstand system tract (HST) in the upper part, separated by the maximum flooding surface.

4.3.1. Characteristics of Sequence Boundaries in the Well. The KT-II carbonate sequences developed on the shallow marine carbonate platform adjacent to the Ural trough in the east and are mainly composed of carbonate shoal deposits in the study area (Figures 2 and 4). The lithology is basically sparry grain limestone, followed by packstones and marl [46, 48]. The GR curve is flat with low values, indicating a low shale content and pure carbonate (Figure 9(b)). Although the KT-II strata are relatively pure limestone overall, the KT-II deposit, which is separated by the second-order sequence boundary, i.e., the unconformity between Bashkirian and Moskovian strata, has changed obviously.

According to the lithology of well A, which was drilled into the CFC, the canyon deposits can be divided into two second-order sequences, Ss1 and Ss2, which are separated by SB1. The lithology of Ss1 is mainly sparry limestone, so the GR curve is straight with a thick box shape. For an increase in the shale content upwards above the sequence boundary, the shape of the logging curves changes obviously, the GR value increases, and the DT value decreases [46, 48] (Figure 10). The main lithology of Ss2 changes into sparry bioclastic limestone, alga-gobbet limestone and mudstone, and muddy micrite limestone [46, 48] (Figure 10). In Ss2, there are three system tracts, and the coarsening-upward HST succession is predominant (Figure 10).

4.3.2. Seismic Sequence Stratigraphic Correlation. Based on the analysis of the sequence division, well correlation, and seismic-well ties of well A drilled into the CFC and other multiple exploration wells in the study area, the sequence boundary was found via several representative seismic lines first and then traced throughout the entire study area.

The carbonate platform of KT-II, showing low-frequency and weak-amplitude reflections (seismic facies 3), is in conformable contact with the underlying middle Visean clastic deposition (seismic facies 5 and 6) (Figures 5 and 8). Canyon fill deposits, which are overlain by platform slope deposits (seismic facies 2), exhibit medium-weak amplitudes and chaotic or subparallel reflections (seismic facies 1) truncated with the surrounding middle Visean clastic deposits (seismic facies 5 and 6), forming a U-shaped canyon basal unconformity (Figure 5).

The sequence boundary is located in the interiors of open platform deposits with intermittent and weak reflections (Figure 5(c)). According to the seismic-well tie analysis between seismic data and well A, the only well in the study area drilled into the CFC, the shale contents of Ss2 carbonate deposits, which are above sequence boundary SB1, are higher compared to those of Ss1 (Figure 10). The CFC was nearly completely filled during Ss1 deposition. The canyon infillings and platform deposits of Ss1 both have low amplitudes and moderate- to low-continuity reflections with canyon infillings that are more chaotic (Figures 5 and 9(a)).

Above the sequence boundary, the open platform deposits are layered deposits with high continuity and parallel seismic reflections (seismic facies 3) (Figures 5 and 9(b)), while towards the CFC, the high-continuity prograding carbonate platform with higher amplitude (seismic facies 4) (Figures 5 and 9(c)), resulting from the sedimentary environment change and increasing shale content, downlaps onto the canyon fill deposits of Ss1.

The RMS map between SB1 and the basal surface of KT-II shows some linear low-amplitude reflections, which are small gullies located in the head segment and one channel each in the middle segment and lower segment in Ss1, delivering sediments into the CFC (Figures 7 and 11(a)). These channels can also be distinguished as dark-coloured linear features in the flattened horizontal coherence slice at 100 m below SB1 (Figure 12(a)).

However, in Ss2, obvious shifts in the position of the platform margin occurred due to westward progradation, which shows large-scale linear low-amplitude reflections in the RMS map between the top surface of KT-II and SB1 (Figure 11(b)). These are channels perpendicular to the slope originating close to the platform edge, which are transported and filled with coarse carbonate debris derived from the platform (Figure 11(b)). The progradation of the platform shows grey-coloured coherence patterns with convex-westward plan-form geometries, as visible in plan view (Figure 12(b)). The development of clinoform geometries crossed the canyon fillings, and the platform margin expanded (Figure 12(b)).

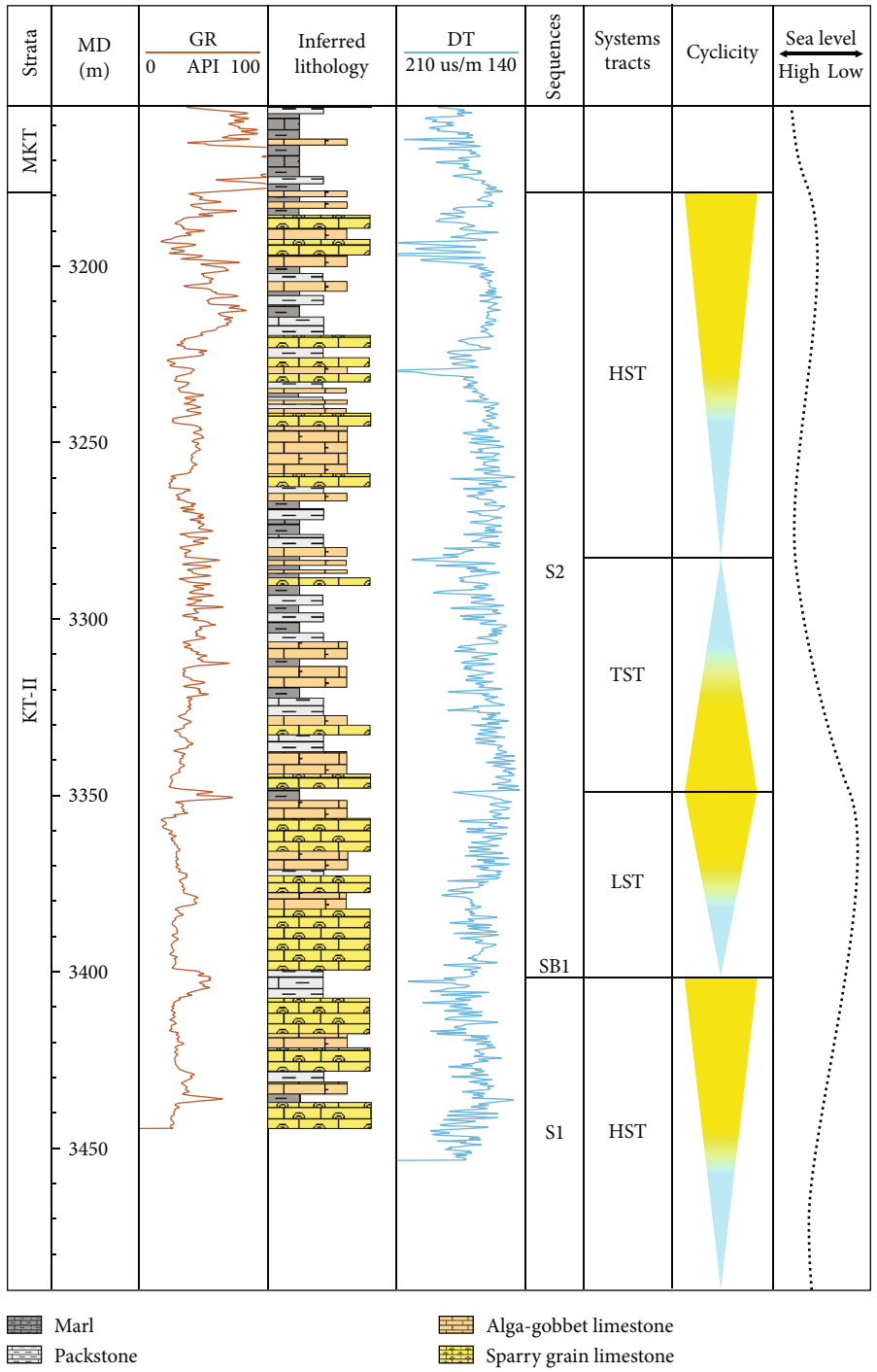

Figure 10: Inferred lithology and stratigraphic architecture within the canyon fill based on integrated logs of well A. See Figure 4 for the well A location. Note that the well does not penetrate the canyon fill sediments but penetrates only the HST of Ss1. HST stands for highstand system tract, TST stands for transgressive system tract, and LST stands for lowstand system tract.

5. Discussion

5.1. Canyon Origin. The canyons reported worldwide are now grouped into three main types: slope-confined canyons (also named blind canyons or headless canyons), whose heads terminate on the slope, and canyons that incise the shelf, which connect with and without a major river system [13, 21, 51]. According to this, the CFC can most likely be defined as a blind canyon. The formation of blind canyons has been explained by fluid seepage-induced slope failure [57], a combination of slope failure and retrogressive erosion [13, 16, 51], and the interplay of downslope processes and along-slope currents [58] that have been recently reported. Although some slope-parallel negative bedforms, such as moat channels, are mainly caused by bottom currents and some canyons and channels are also controlled by along-

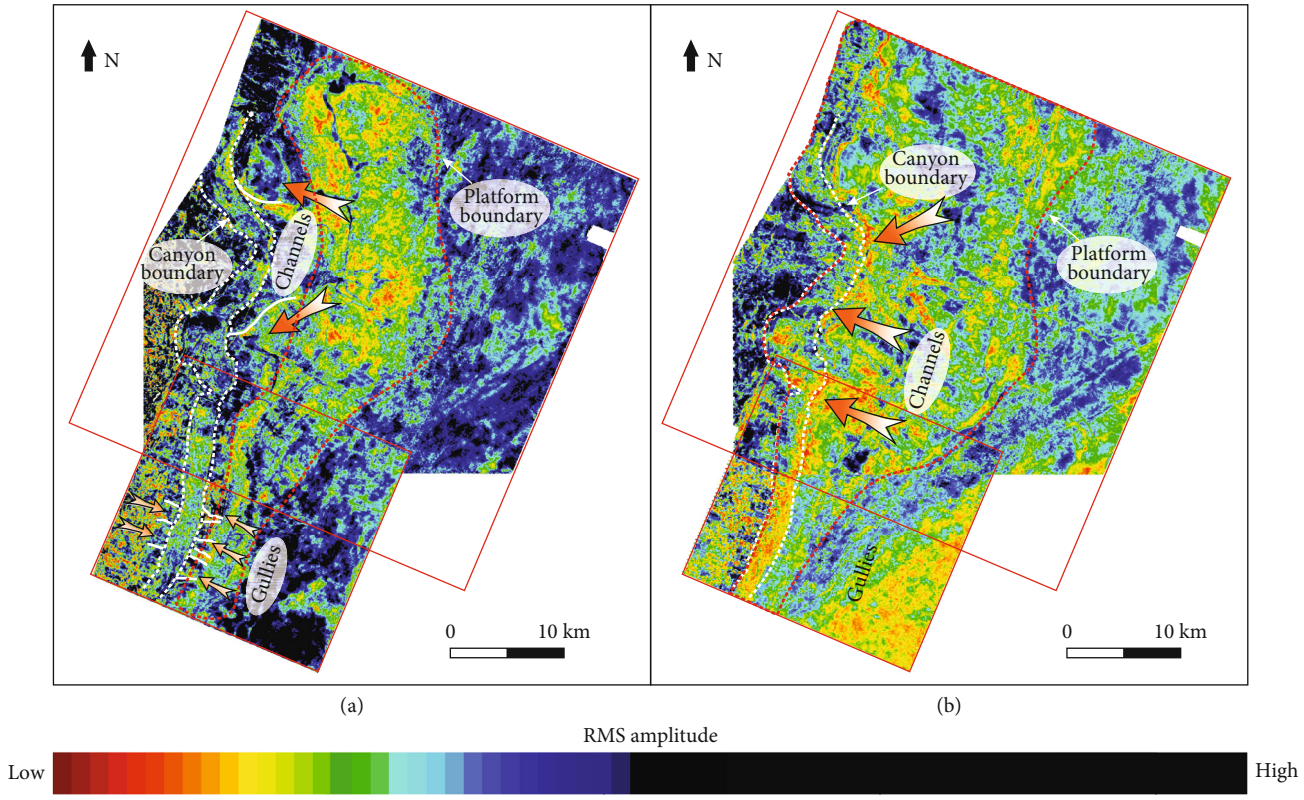

Figure 11: (a) RMS amplitude map between SB1 and the basal surface of KT-II. A series of small gullies are located in the head segment of the CFC, and two channels are located in the middle and lower segments, with low RMS amplitude values. (b) RMS amplitude map between SB1 and the top surface of KT-II. Some large-scale channels perpendicular to the slope originating close to the platform edge are dominated by low RMS values. See the position in Figure 2.

slope sedimentary processes in addition to downslope gravity processes [35, 36, 59–61], there is now no obvious evidence that the CFC has a direct connection with fluvial systems and bottom currents, so the most likely formation mechanism of the CFC is upslope erosion through headward retrogressive mass failures.

Due to the collision of the Kazakh and European plates, the Uralian orogeny began to develop in the early-mid-Visean and early Carboniferous, on the eastern flank of the Precaspian Basin [38, 41], and the eastern margin of the Precaspian Basin was gradually compressed and uplifted, which had an important impact on the palaeogeomorphology of the study area. The structure of KT-II was modified by later tectonic activities, and the cast method [62, 63] was used to restore the palaeogeomorphology before the deposition of the CFC with two selected reference interfaces: the top of the MKT and the bottom of the canyon and bottom of KT-II (Figure 13). For minor erosion in the 3D seismic survey, the resultant cast map can be used to interpret the relative relief of the palaeogeomorphology before the deposition of the CFC.

A confined elongated negative relief parallel to the following KT-II carbonate platform was formed between the uplifts due to the compressional orogeny (Figure 13). Geomorphic factors have a very important influence on the development and evolution of the canyon [18–21, 64], and the canyon was easily formed in the area limited by the uplifts on both sides. In addition, the uplift in the middle of the 3D survey remained topographically high enough to provide proper environments conducive for shallow-water carbonate platform production. For instance, carbonate factories developed on submerged structural highs in the Isili Basin [30]. For the low sea level in late Visean and the confined geomorphology, the CFC was initiated to form the canyon origin, which favoured the funnelling of sediments originating from the platform [14, 65]. Subsequently, or contemporaneously with upslope headward retreat and incision, turbidity currents promoted the formation of the canyon [40, 66].

As the slope gradient of the head segment was gentle, the turbidity currents had the lowest erosional ability [67, 68], so this part is obviously shallower than the middle segment and lower segment due to the limited incision (Figure 6). In the middle segment, the depth and width of the canyon apparently increase. Owing to the steepest average slope gradient and the existence of the "waterfall" at knickpoint 1, the erosive currents had higher flow velocities and erosional ability. At the start of the middle segment, with the gradual increase in the canyon depth, the trend of the canyon changed sharply from NNE to NW (Figures 4 and 6), which led to turbidity currents flowing towards the canyon walls and increasing lateral erosion; therefore, the curvature of the middle segment increased. In the lower segment of the canyon, the velocities and erosive capacities of turbidity currents

Figure 12: (a) Coherence slice along the surface 100 m below flattened SB1. The gullies and channels display a dark-coloured coherence pattern, and the canyon fill deposits exhibit a grey-coloured coherence pattern. (b) Coherence slice along the surface, which is 100 m shallower than flattened SB1. The progradation of the platform shows a grey-coloured coherence pattern with convex-westward planform geometries, as visible in plan view. See the position in Figure 4.

would be the highest for the energy accumulation in the upper two segments. Therefore, the lower segment is the deepest with the highest sinuosity, although the slope gradient is the slowest (Figure 6).

Faults always play an important role in the formation and evolution of a canyon [17, 69]. Due to the plate collision of the eastern edge of the basin [37, 41, 42], reverse faults are developed in the study area (Figures 5(a)–5(d)). The ESP map shown at 50 m below the canyon bottom in plan view and vertical seismic profiles across the CFC both show that the canyon is bounded by two continuous reverse faults (Figure 7(b)). For regional compression, fractures and small faults are rich in the anticline between the two reverse faults, which reduces the strength of the stratum and makes it more vulnerable to weathering and denudation. Thus, faults are a favourable factor for canyon formation. For the same reason, the width of the canyon is closely related to faulting. According to the seismic profiles, the widest part of the middle segment has very developed underlying faults where the strata were more easily eroded, so the middle segment is the widest in the CFC (Figure 6). In addition, it is noteworthy that the width and depth of the CFC decrease abruptly at the junction points between segments (Figure 6). This is attributed to the fewer faults at these two knickpoints, which are shown in both the coherence slice and seismic profile (Figures 5(e), 7, and 12). The seismic facies of knickpoints are the same as

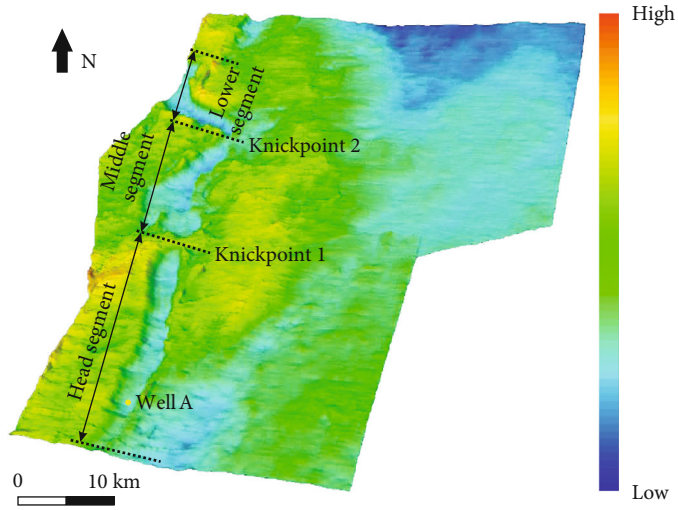

Figure 13: Restored palaeogeomorphologic map before the deposition of the CFC. A confined elongated negative relief was formed between the uplifts.

those of the underlying early Visean strata (Figure 5(e)), which have moderate amplitudes with high-continuity parallel reflections. The formation was difficult to erode due to undeveloped fractures, thus forming these two knickpoints, which are similar to two small crests dividing the CFC into three segments.

5.2. Canyon Filling Processes. During the deposition of the highstand system tract in Ss1, the carbonate platform grew vertically, resulting in low-amplitude and high-continuity parallel reflections (seismic facies 2) (Figure 5). When the sea level rose to a highstand, the productivity of the carbonate factory greatly increased with much carbonate deposition, especially in the carbonate platform interior, which was mainly in the leeward direction and favoured carbonate sedimentation [65, 70]. The slope instability increased for the prior vertical accretion, which promoted the delivery of carbonate debris downslope. Combined with sea level lowering, the carbonate factory moved closer to the slope break of the platform and destabilized sediments by increased porewater pressure [65, 71]. During this stage, the sediments of the carbonate platform were transported mainly by channels or small gullies on both sides of the platform (Figures 11(a) and 12(a)). The original confined negative topography accumulated sediments from the platform and served as a conduit to promote the formation and development of the CFC [14, 65]. However, with the gradual increase in platform productivity, increasingly more sediments were deposited in the CFC and almost filled it (Figure 5).

The lower sea level of the lowstand system tract of Ss2 caused low productivity of the carbonate factory. When the relative sea level rose to a highstand during the transgressive and highstand system tracts, the productivity of the carbonate factory greatly increased. The carbonate platform accelerated to expand laterally through progradation into the former platform interior with downlap on the canyon fill deposits (Figures 5, 11(b), and 12(b)). Platform progradation and merging of separate platforms always occur by this kind of lateral accretion. Similar occurrences have been documented in the middle Miocene prograding carbonate bank margins of the Maldives [72] and the Miocene-Pliocene Segitiga platform in Indonesia [55].

5.3. Evolutionary Stages of the CFC. Based on the above analysis, a schematic illustration of the depositional processes of the CFC in the Carboniferous KT-II at the eastern edge of the Precaspian Basin was established (Figure 14).

5.3.1. Incising Stage. Due to the collision of the Kazakh and European plates, the confined elongated negative palaeogeomorphology formed, and reverse faults developed in the study area in the late Visean (Figures 5 and 13). The reverse faults weakened the strength of the strata in the confined palaeogeomorphology. Combined with the low sea level of the LST of Ss1, the canyon is formed by incision of the original negative relief through headward retrogressive mass failures during the incising stage (Figure 14(a)). The uplift provided proper environments for shallow-water carbonate platform production, so during this stage, the sediments from the platform promoted the formation and development of the CFC.

5.3.2. Early Filling Stage. During this stage, for the rising sea level of the TST and HST in Ss1, the productivity of the carbonate factory greatly increased, especially in the leeward direction. Channels and gullies perpendicular to the canyon walls delivered platform sediments into the CFC (Figures 11(a) and 12(a)). First, the CFC was deepened, and as more sediments were supplied, the CFC was nearly filled at the end of this stage (Figure 14(b)).

5.3.3. Late Filling Stage. As the CFC was basically filled in the former stage, the overall terrain was relatively flat in the platform interior. Because the sea level almost kept rising during the late filling stage of Ss2, the carbonate platform expanded into the former platform interior through progradation clinoforms (Figures 11(b) and 12(b)). After this stage, the CFC was completely filled, and the negative relief was gone (Figure 14(c)).

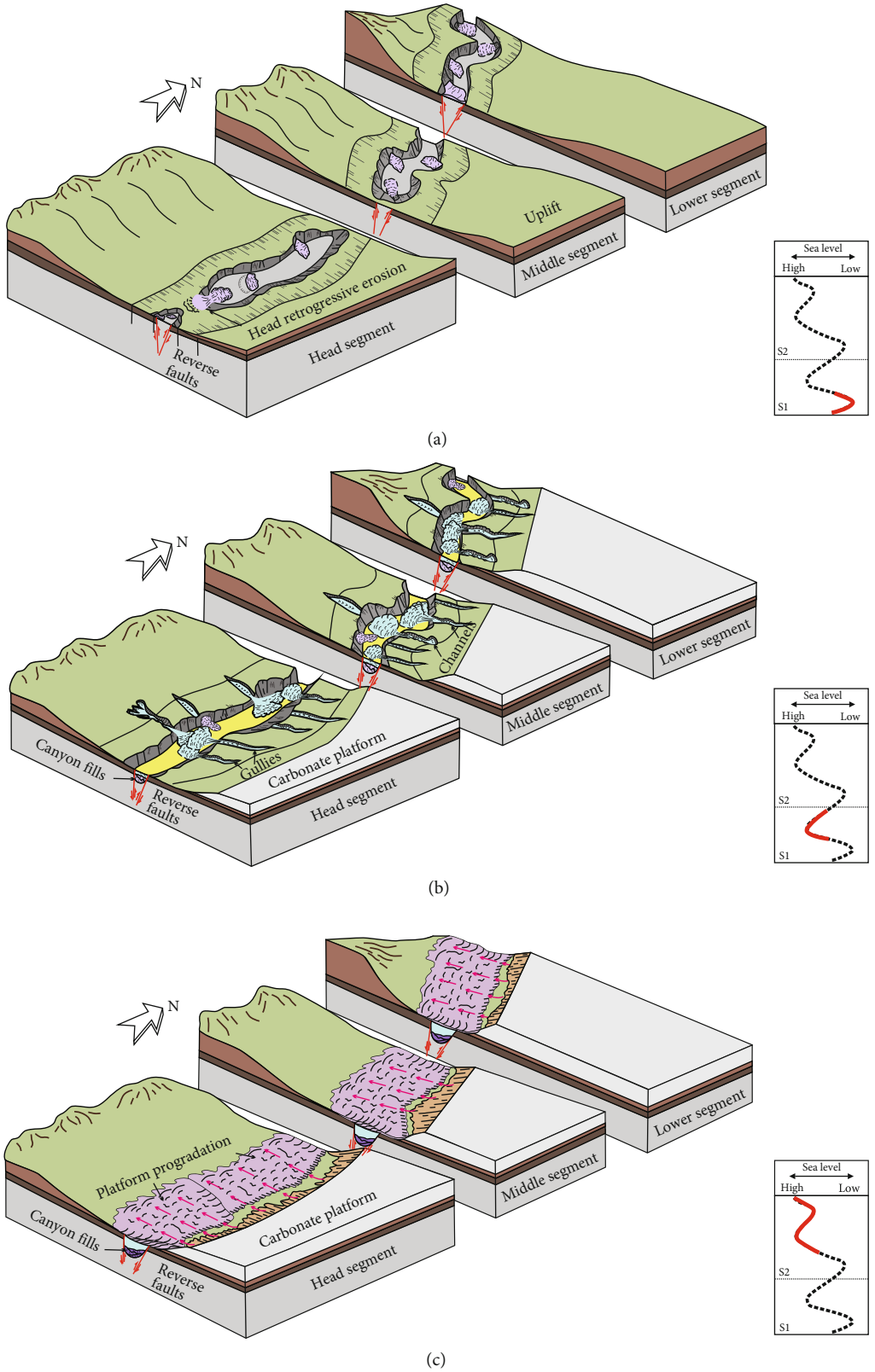

Figure 14: Depositional model summarizing the filling process and depositional architecture of the carbonate-filled canyon. There are three evolution stages: (a) incising stage; (b) early filling stage, when the sediments mainly originated from the platform and were transported through gullies and channels; and (c) late filling stage, during which the canyon was filled by platform progradation. See the text in Section 5.3 for a detailed description.

Overall, the palaeogeomorphology and faults caused by tectonic movement controlled the formation and geomorphic characteristics of the CFC, while variations in the amount and sediment supply influenced by sea level change controlled the infilling process of the CFC.

6. Conclusions

The CFC at the eastern edge of the Precaspian Basin showed a N-S orientation and S-shaped geometry and was parallel to the open carbonate platform of KT-II. The whole CFC was divided into three segments by two knickpoints from south to north for changes in the incision depth and width. For the palaeogeomorphology and faults induced by regional compressional movement, the CFC formed along the thalweg of a confined palaeotopographic feature during early Carboniferous times.

Six kinds of seismic facies were identified in the canyon. The sedimentary interpretations of CFC-related sediments were carried out by combining logging and core data. This, together with planar attribute analysis, such as RMS, leads to distinguishing three stages of the evolution of the canyon: the incising stage, the early filling stage, and the late filling stage. During the incising stage, the confined negative relief and reverse faults caused by tectonic activity, combined with the low sea level, all contributed to the initiation of the CFC and development through headward retrogressive mass failures. During the subsequent early filling stage, much carbonate sediment was produced by the carbonate factory and transported into the CFC by channels and gullies perpendicular to the platform. The CFC was nearly filled by the end of this stage. Finally, during the rising sea level and geomorphic change, the canyon fillings were dominated by platform progradation in the late filling stage. In summary, tectonics controlled the formation of the CFC, while sedimentary processes contributed to its excavation and infilling.

Data Availability

The data used to support the findings of this study are included within the supplementary information file(s).

Conflicts of Interest

The authors declare that there is no conflict of interest regarding the publication of this paper.

Acknowledgments

We would like to acknowledge CNODC for providing and permitting the publication of the geological data. The work was supported by the Science and Technology Project of China National Petroleum Corporation (grant number 2021DJ3402) and Science and Technology Project of China National Logging Corporation (grant numbers CNLC2022-10D02, CNLC2022-10D03, and CPL2021-D04).

Supplementary Materials

We provide Figure 6 and its data in PDF format. *(Supplementary Materials)*

References

[1] A. A. Antobreh and S. Krastel, "Morphology, seismic characteristics and development of Cap Timiris Canyon, offshore Mauritania: a newly discovered canyon preserved-off a major arid climatic region," *Marine and Petroleum Geology*, vol. 23, no. 1, pp. 37–59, 2006.

[2] N. Babonneau, B. Savoye, M. Cremer, and B. Klein, "Morphology and architecture of the present canyon and channel system of the Zaire deep-sea fan," *Marine and Petroleum Geology*, vol. 19, no. 4, pp. 445–467, 2002.

[3] J. Laursen and W. R. Normark, "Late Quaternary evolution of the San Antonio submarine canyon in the central Chile forearc (~33°S)," *Marine Geology*, vol. 188, no. 3-4, pp. 365–390, 2002.

[4] C. M. G. McHugh, J. E. Damuth, and G. S. Mountain, "Cenozoic mass-transport facies and their correlation with relative sea-level change, New Jersey continental margin," *Marine Geology*, vol. 184, no. 3-4, pp. 295–334, 2002.

[5] I. Popescu, G. Lericolais, N. Panin, A. Normand, C. Dinu, and E. Le Drezen, "The Danube submarine canyon (Black Sea): morphology and sedimentary processes," *Marine Geology*, vol. 206, no. 1-4, pp. 249–265, 2004.

[6] A. H. Bouma, "Fine-grained submarine fans as possible recorders of long- and short-term climatic changes," *Global and Planetary Change*, vol. 28, no. 1-4, pp. 85–91, 2001.

[7] F. X. Gingele, P. De Deckker, and C.-D. Hillenbrand, "Late Quaternary terrigenous sediments from the Murray canyons area, offshore South Australia and their implications for sea level change, palaeoclimate and palaeodrainage of the Murray–Darling basin," *Marine Geology*, vol. 212, no. 1-4, pp. 183–197, 2004.

[8] M. Umar, A. S. Khan, G. Kelling, and A. M. Kassi, "Depositional environments of Campanian–Maastrichtian successions in the Kirthar fold belt, southwest Pakistan: tectonic influences on late cretaceous sedimentation across the Indian passive margin," *Sedimentary Geology*, vol. 237, no. 1-2, pp. 30–45, 2011.

[9] F. F. Vesely, B. Trzaskos, F. Kipper, M. L. Assine, and P. A. Souza, "Sedimentary record of a fluctuating ice margin from the Pennsylvanian of western Gondwana: Paraná Basin, southern Brazil," *Sedimentary Geology*, vol. 326, pp. 45–63, 2015.

[10] J. P. Wonham, S. Jayr, R. Mougamba, and P. Chuilon, "3D sedimentary evolution of a canyon fill (Lower Miocene-age) from the Mandorove formation, offshore Gabon," *Marine and Petroleum Geology*, vol. 17, no. 2, pp. 175–197, 2000.

[11] S.-C. Fuh, C.-C. Chern, S.-C. Liang et al., "The biogenic gas potential of the submarine canyon systems of Plio-Peistocene foreland basin, southwestern Taiwan," *Marine and Petroleum Geology*, vol. 26, no. 7, pp. 1087–1099, 2009.

[12] M. Mayall, E. Jones, and M. Casey, "Turbidite channel reservoirs—key elements in facies prediction and effective development," *Marine and Petroleum Geology*, vol. 23, no. 8, pp. 821–841, 2006.

[13] P. T. Harris and T. Whiteway, "Global distribution of large submarine canyons: geomorphic differences between active and passive continental margins," *Marine Geology*, vol. 285, no. 1-4, pp. 69–86, 2011.

[14] E. Tournadour, T. Mulder, J. Borgomano et al., "Submarine canyon morphologies and evolution in modern carbonate settings: the northern slope of Little Bahama Bank, Bahamas," *Marine Geology*, vol. 391, pp. 76–97, 2017.

[15] N. F. Exon, P. J. Hill, C. Mitchell, and A. Post, "Nature and origin of the submarine Albany canyons off southwest Australia," *Australian Journal of Earth Sciences*, vol. 52, no. 1, pp. 101–115, 2005.

[16] Z. R. Jobe, D. R. Lowe, and S. J. Uchytil, "Two fundamentally different types of submarine canyons along the continental margin of Equatorial Guinea," *Marine and Petroleum Geology*, vol. 28, no. 3, pp. 843–860, 2011.

[17] C. Gong, Y. Wang, W. Zhu, W. Li, Q. Xu, and J. Zhang, "The central submarine canyon in the Qiongdongnan Basin, northwestern South China Sea: architecture, sequence stratigraphy, and depositional processes," *Marine and Petroleum Geology*, vol. 28, no. 9, pp. 1690–1702, 2011.

[18] C. Li, M. Ma, C. Lv et al., "Sedimentary differences between different segments of the continental slope-parallel central canyon in the Qiongdongnan Basin on the northern margin of the South China Sea," *Marine and Petroleum Geology*, vol. 88, pp. 127–140, 2017.

[19] X. Li, L. Fairweather, S. Wu et al., "Morphology, sedimentary features and evolution of a large palaeo submarine canyon in Qiongdongnan basin, northern South China Sea," *Journal of Asian Earth Sciences*, vol. 62, pp. 685–696, 2013.

[20] C. Liang, X. Xie, Y. He et al., "Multiple sediment sources and topographic changes controlled the depositional architecture of a palaeoslope-parallel canyon in the Qiongdongnan Basin, South China Sea," *Marine and Petroleum Geology*, vol. 113, article 104161, 2020.

[21] M. Su, X. Xie, Y. Xie et al., "The segmentations and the significances of the central canyon system in the Qiongdongnan Basin, northern South China Sea," *Journal of Asian Earth Sciences*, vol. 79, pp. 552–563, 2014.

[22] T. Mulder, H. Gillet, V. Hanquiez et al., "Into the deep: a coarse-grained carbonate turbidite valley and canyon in ultra-deep carbonate setting," *Marine Geology*, vol. 407, pp. 316–333, 2019.

[23] C. Betzler, M. Pfeiffer, and S. Saxena, "Carbonate shedding and sedimentary cyclicities of a distally steepened carbonate ramp (Miocene, Great Bahama Bank)," *International Journal of Earth Sciences*, vol. 89, no. 1, pp. 140–153, 2000.

[24] C. Betzler, J. J. G. Reijmer, K. Bernet, G. P. Eberli, and F. S. Anselmetti, "Sedimentary patterns and geometries of the Bahamian outer carbonate ramp (Miocene–Lower Pliocene, Great Bahama Bank)," *Sedimentology*, vol. 46, no. 6, pp. 1127–1143, 1999.

[25] S. Gallagher, A. J. Smith, K. Jonasson et al., "The Miocene palaeoenvironmental and palaeoceanographic evolution of the Gippsland Basin, Southeast Australia: a record of Southern Ocean change," *Palaeogeography Palaeoclimatology Palaeoecology*, vol. 172, no. 1-2, pp. 53–80, 2001.

[26] G. Holdgate, M. Wallace, J. Daniels, S. Gallagher, J. B. Keene, and A. J. Smith, "Controls on Seaspray Group sonic velocities in the Gippsland Basin-a multi-disciplinary approach to the canyon seismic velocity problem," *The APPEA Journal*, vol. 40, no. 1, Part 1, pp. 293–312, 2000.

[27] M. W. Wallace, G. R. Holdgate, J. Daniels, S. J. Gallagher, and A. Smith, "Sonic velocity, submarine canyons, and burial diagenesis in Oligocene-Holocene cool-water carbonates, Gippsland Basin, Southeast Australia," *AAPG Bulletin*, vol. 86, pp. 1593–1607, 2002.

[28] M. A. Brown, A. W. Archer, and E. P. Kvale, "Neap-spring tidal cyclicity in laminated carbonate channel-fill deposits and its implications; Salem limestone (Mississippian), south-central Indiana, USA," *Journal of Sedimentary Research*, vol. 60, no. 1, pp. 152–159, 1990.

[29] E. C. Rankey, "Carbonate-filled channel complexes on carbonate ramps: an example from the Peerless Park member [Keokuk limestone, Visean, Lower Carboniferous (Mississippian)], St. Louis, MO, USA," *Sedimentary Geology*, vol. 155, no. 1-2, pp. 45–61, 2003.

[30] M. Vigorito, M. Murru, and L. Simone, "Anatomy of a submarine channel system and related fan in a foramol/rhodalgal carbonate sedimentary setting: a case history from the Miocene syn-rift Sardinia Basin, Italy," *Sedimentary Geology*, vol. 174, no. 1-2, pp. 1–30, 2005.

[31] Y. He, X. Xie, B. C. Kneller, Z. Wang, and X. Li, "Architecture and controlling factors of canyon fills on the shelf margin in the Qiongdongnan Basin, northern South China Sea," *Marine and Petroleum Geology*, vol. 41, pp. 264–276, 2013.

[32] J. Peakall and E. J. Sumner, "Submarine channel flow processes and deposits: a process-product perspective," *Geomorphology*, vol. 244, pp. 95–120, 2015.

[33] H. W. Posamentier and V. Kolla, "Seismic geomorphology and stratigraphy of depositional elements in deep-water settings," *Journal of Sedimentary Research*, vol. 73, no. 3, pp. 367–388, 2003.

[34] Z. Sylvester, C. Pirmez, and A. Cantelli, "A model of submarine channel-levee evolution based on channel trajectories: implications for stratigraphic architecture," *Marine and Petroleum Geology*, vol. 28, no. 3, pp. 716–727, 2011.

[35] W. Zhou, Y. Wang, X. Gao et al., "Architecture, evolution history and controlling factors of the Baiyun submarine canyon system from the middle Miocene to Quaternary in the Pearl River Mouth Basin, northern South China Sea," *Marine and Petroleum Geology*, vol. 67, pp. 389–407, 2015.

[36] M. Zhu, S. Graham, X. Pang, and T. McHargue, "Characteristics of migrating submarine canyons from the middle Miocene to present: implications for paleoceanographic circulation, northern South China Sea," *Marine and Petroleum Geology*, vol. 27, no. 1, pp. 307–319, 2010.

[37] J.-P. Barde, P. Gralla, J. Harwijanto, and J. Marsky, "Exploration at the eastern edge of the Precaspian Basin: impact of data integration on upper Permian and Triassic prospectivity," *AAPG Bulletin*, vol. 86, pp. 399–415, 2002.

[38] O. B. Duffy, N. Fernandez, M. R. Hudec et al., "Lateral mobility of minibasins during shortening: insights from the SE Precaspian Basin, Kazakhstan," *Journal of Structural Geology*, vol. 97, pp. 257–276, 2017.

[39] Z. Wu, H. Yin, X. Wang et al., "The structural styles and formation mechanism of salt structures in the southern Precaspian Basin: insights from seismic data and analog modeling," *Marine and Petroleum Geology*, vol. 62, pp. 58–76, 2015.

[40] N. M. de Almeida, H. Vital, and M. P. Gomes, "Morphology of submarine canyons along the continental margin of the Potiguar Basin, NE Brazil," *Marine and Petroleum Geology*, vol. 68, pp. 307–324, 2015.

[41] N. Fernandez, O. B. Duffy, M. R. Hudec et al., "The origin of salt-encased sediment packages: observations from the SE Precaspian Basin (Kazakhstan)," *Journal of Structural Geology*, vol. 97, pp. 237–256, 2017.

[42] S. Wang, L. Zhao, X. Cheng, Z. Fan, and L. He, "Geochemical characteristics and genetic model of dolomite reservoirs in the eastern margin of the Pre-Caspian Basin," *Petroleum Science*, vol. 9, no. 2, pp. 161–169, 2012.

[43] Y. Volozh, C. Talbot, and A. Ismail-Zadeh, "Salt structures and hydrocarbons in the Pricaspian Basin," *AAPG Bulletin*, vol. 87, no. 2, pp. 313–334, 2003.

[44] Y. A. Volozh, M. P. Antipov, M.-F. Brunet, I. Garagash, L. I. Lobkovskii, and J.-P. Cadet, "Pre-Mesozoic geodynamics of the Precaspian Basin (Kazakhstan)," *Sedimentary Geology*, vol. 156, no. 1-4, pp. 35–58, 2003.

[45] M.-F. Brunet, Y. Volozh, M. Antipov, and L. Lobkovsky, "The geodynamic evolution of the Precaspian Basin (Kazakhstan) along a north–south section," *Tectonophysics*, vol. 313, no. 1-2, pp. 85–106, 1999.

[46] D. Zhang, *Study on Sedimentary Facies of Southeastern of Precaspian Basin, [M.S. Thesis]*, China University of Geosciences, 2016.

[47] J. Fang, L. Wu, G. Gao, and B. Zhao, "Sedimentary facies and types of carbonate rock reservoir in Caspian Seashore Basin: a case from Carboniferous KT-II memeber in Zahnanor oilfield," *Petroleum Exploration and Development*, vol. 35, pp. 498–508, 2008.

[48] S. Yin, W. Huang, Z. Jin, and B. Gao, "Characteristics of carbonate microfacies and sedimentary environment of the east margin of Caspian Basin in the Carboniferous KT-II layer: a case from Zanazor area," *Acta Sedimentologica Sinica*, vol. 35, pp. 139–150, 2017.

[49] Y. Tian, *Study on sequences stratigraphy and sedimentary facies of mid-block, eastern of Precaspian Basin, [M.S. thesis]*, China University of Geosciences, Beijing, 2011.

[50] V. Catterall, J. Redfern, R. Gawthorpe, D. Hansen, and M. Thomas, "Architectural style and quantification of a submarine channel–levee system located in a structurally complex area: offshore Nile Delta," *Journal of Sedimentary Research*, vol. 80, no. 11, pp. 991–1017, 2010.

[51] Z. Huang, S. L. Nichol, P. T. Harris, and M. J. Caley, "Classification of submarine canyons of the Australian continental margin," *Marine Geology*, vol. 357, pp. 362–383, 2014.

[52] B. Ma, Z. Qin, S. Wu et al., "High-resolution acoustic data revealing peri-platform sedimentary characteristics in the Xisha Archipelago South China Sea," *Interpretation*, vol. 9, no. 2, pp. T533–T547, 2021.

[53] C. C. Mitchell, "Interpreting long-profiles of canyons in the USA Atlantic continental slope," *Marine Geology*, vol. 214, no. 1-3, pp. 75–99, 2005.

[54] X. Wang, F. Cai, Z. Sun et al., "Tectonic and oceanographic controls on the slope-confined dendritic canyon system in the Dongsha Slope, South China Sea," *Geomorphology*, vol. 410, article 108285, 2022.

[55] S. L. Bachtel, R. D. Kissling, D. Martono, S. P. Rahardjanto, P. A. Dunn, and B. A. MacDonald, "Seismic stratigraphic evolution of the Miocene-Pliocene Segitiga platform, East Natuna Sea, Indonesia: the origin, growth, and demise of an isolated carbonate platform," *AAPG Memoir*, vol. 81, pp. 309–328, 2004.

[56] C. Octavian, V. Abreu, J. Bhattacharya et al., "Towards the standardization of sequence stratigraphy," *Earth-Science Reviews*, vol. 92, no. 1-2, pp. 1–33, 2009.

[57] D. L. Orange and N. A. Breen, "The effects of fluid escape on accretionary wedges 2. Seepage force, slope failure, headless submarine canyons, and vents," *Journal of Geophysical Research: Solid Earth*, vol. 97, no. B6, pp. 9277–9295, 1992.

[58] G. Warratz, T. Schwenk, I. Voigt et al., "Interaction of a deep-sea current with a blind submarine canyon (Mar del Plata Canyon, Argentina)," *Marine Geology*, vol. 417, article 106002, 2019.

[59] C. Gong, Y. Wang, R. J. Steel, J. Peakall, X. Zhao, and Q. Sun, "Flow processes and sedimentation in unidirectionally migrating deep-water channels: from a three-dimensional seismic perspective," *Sedimentology*, vol. 63, no. 3, pp. 645–661, 2016.

[60] H. Li, Y. Wang, W. Zhu et al., "Seismic characteristics and processes of the Plio-Quaternary unidirectionally migrating channels and contourites in the northern slope of the South China Sea," *Marine and Petroleum Geology*, vol. 43, pp. 370–380, 2013.

[61] E. Marchès, T. Mulder, M. Cremer et al., "Contourite drift construction influenced by capture of Mediterranean outflow water deep-sea current by the Portimão submarine canyon (Gulf of Cadiz, South Portugal)," *Marine Geology*, vol. 242, no. 4, pp. 247–260, 2007.

[62] R. Martin, "Paleogeomorphology and its application to exploration for oil and gas (with examples from Western Canada)," *AAPG Bulletin*, vol. 50, pp. 2277–2311, 1966.

[63] H. Zeng, W. Zhao, Z. Xu et al., "Carbonate seismic sedimentology: a case study of Cambrian Longwangmiao formation, Gaoshiti-Moxi area, Sichuan Basin, China," *Petroleum Exploration and Development*, vol. 45, no. 5, pp. 830–839, 2018.

[64] D. Gamboa, T. M. Alves, and J. Cartwright, "A submarine channel confluence classification for topographically confined slopes," *Marine and Petroleum Geology*, vol. 35, no. 1, pp. 176–189, 2012.

[65] A. Payros and V. Pujalte, "Calciclastic submarine fans: an integrated overview," *Earth-Science Reviews*, vol. 86, no. 1-4, pp. 203–246, 2008.

[66] I. R. Clark and J. A. Cartwright, "Key controls on submarine channel development in structurally active settings," *Marine and Petroleum Geology*, vol. 28, no. 7, pp. 1333–1349, 2011.

[67] B. Kneller, "The influence of flow parameters on turbidite slope channel architecture," *Marine and Petroleum Geology*, vol. 20, no. 6-8, pp. 901–910, 2003.

[68] Z. Wang, H. Zhuo, Y. Wang et al., "Controls of contour currents on intra-canyon mixed sedimentary processes: insights from the Pearl River canyon, northern South China Sea," *Marine Geology*, vol. 406, pp. 193–213, 2018.

[69] L. Rinke-Hardekopf, L. Reuning, J. Bourget, and S. Back, "Synsedimentary deformation as a mechanism for the initiation of submarine gullies on a carbonate platform to slope transition, Browse Basin, Australian north west shelf," *Marine and Petroleum Geology*, vol. 91, pp. 622–630, 2018.

[70] J. W. Counts, S. J. Jorry, E. Leroux, E. Miramontes, and G. Jouet, "Sedimentation adjacent to atolls and volcano-cored carbonate platforms in the Mozambique Channel (SW Indian Ocean)," *Marine Geology*, vol. 404, pp. 41–59, 2018.

[71] B. Ma, S. Wu, L. Mi, T. Lüdmann, J. Gao, and W. Gao, "Mixed carbonate-siliciclastic deposits in a channel complex in the northern South China Sea," *Journal of Earth Science*, vol. 29, no. 3, pp. 707–720, 2018.

[72] A. Belopolsky and A. Droxler, "Seismic expressions of prograding carbonate bank margins: middle Miocene, Maldives, Indian Ocean," *AAPG Memoir*, vol. 81, 2004.